Synthesis and characterization of 2,6-NDC zirconium MOF

Dag Kristian Sannes

Sixty ECTS credits

Master thesis in Chemistry

Department of Chemistry

Faculty of Mathematics and Natural Sciences

UNIVERSITY OF OSLO

June 2020

Acknowledgments

This thesis is the result of experimental work performed at the Department of Chemistry, University of Oslo from August 2018 to June 2020 under the supervision of prof. Karl Peter Lillerud.

I want to start by thanking Karl Peter Lillerud, you were always accessible for any questions I might have had. Without your help and guidance, this thesis would not have been possible.

I would like to thank the MOF office for all the experimental help during this thesis.

Finally, yet importantly, I would like to thank my family. You have always supported me in my endeavors and for that I'm extremely grateful.

2020

Synthesis and characterization of 2,6-NDC zirconium MOF

Dag Sannes

http://www.duo.uio.no/

Trykk: Reprosentralen, Universitetet i Oslo

Abstract

Metal organic frameworks (MOFs) are hybrid three-dimensional crystalline materials built from inorganic metal ions or metal clusters connected with multidentate organic linkers. MOFs are interesting materials because of its high surface area and easily tunable chemistry. The extensive toolkit developed for synthetic organic chemistry can be utilized to simply change the organic linkers both before the assembly of the MOF but also on the crystalline solid. MOFs are excellent materials for application in molecule adsorption and separation, electrochemistry, drug delivery and catalysis, [1, 2]

One challenge with metal organic frameworks is their low thermal, chemical and mechanical stability. A relatively new group of MOFs discovered at University of Oslo (UiO) in 2008, is receiving enormous attention due to its superior thermal, chemical and mechanical stability compared to other types of MOFs [3].

The major experimental work in this thesis has been the synthesis of zirconium 2,6-naphthalene dicarboxylic (2,6-NDC) MOF, one of the least studied members of the UiO- Zr-MOF family. Missing linker and missing cluster defects have been observed and characterized for the zirconium 2,6-NDC MOF. The stability of the 2,6-NDC MOF in high humidity have been compared to UiO-66 and UiO-67. The major characterization tools have been powder X – ray diffraction, thermogravimetric analysis, nitrogen adsorption, nuclear magnetic resonance and scanning electron microscope.

Abbreviations used in this thesis

MOF	Metal Organic Framwork
2,6-NDC	2,6 – Naphthalenedicarboxylic acid
PSM	Post-synthetic modification
UNFCCC	United nations framework convention on climate change
HSSAB	Hard/soft acid/base
FCC	Face center cubic
PSDE	Post-synthetic defect exchange
XRD	X-ray diffraction
pXRD	Powder X-ray diffraction
TGA	Thermogravimetric analysis
DSC	Differential scanning calorimetry
BET	Braunauer – Emmet – Teller
Ls - NMR	Liquid state – Nuclear magnetic resonance
^{1}H-NMR	Hydrogen – Nuclear magnetic resonance
DMF	N,N - dimethylformamide
SEM	Scanning electron microscope
BSE	Back scattered electrons
SE	Secondary electrons
EDX	Energy dispersive X-ray spectroscopy
PSE	Post-syntethic ligand exchange

Contents

1. Introduction

1.1. Background of Metal Organic Frameworks

The term metal organic framework (MOF) was first coined by Yaghi in 1995 [4]. MOFs have since developed into a major research field for both scientific and practical purposes. MOFs can be classified into four groups, referred to as 1st, 2nd, 3rd or 4th generation. The requirement of each group is listed below [5].

> 1st generation: "MOFs have only nonpermanent porosity because of inseparable host–guest dependence, which has often been observed in MOFs containing charged frameworks with pores filled by counter anions."
>
> 2nd generation: "MOFs possess stable and robust porosity against guest removal, typical of neutral and zeolite-like MOFs."
>
> 3rd generation: "MOFs display framework flexibility and dynamics, being able to respond to guest exchange or external stimuli."
>
> 4th generation: "The 4th generation MOFs are correlated to the recently developed post-synthetic modifications (PSM) of MOFs and may be broadly defined as post-processing MOFs which can maintain underlying topology and structural integrity towards various post-modifications."

1.1.1. 1st generation metal organic frameworks

The 1st generation MOFs lose their porosity if the host guests are removed. These materials have naturally very few practical applications. A major research effort has been devoted to the synthesis of MOFs that would retain their surface area after guest removal.

1.1.2. 2nd generation metal organic frameworks

The first 2nd generation MOF was first reported by Yaghi et al. in Nature in 1999. This material remained crystalline after guest molecule removal and was thermally stable up to 300 ℃. This groundbreaking material was named MOF – 5. MOF - 5 is built up of $Zn_4(O)$ clusters connected to six dicarboxylate linkers [6].

1.1.3. 3rd generation metal organic frameworks

3rd generations MOFs are flexible, meaning that once the inorganic nodes are assembled with organic spacers into a crystalline state, there are still flexibility in the structure. this generation of MOFs are in general guest – responsive which increase the selectivity of the material [7].

1.1.4. 4th generation metal organic frameworks

A 4th generation MOF can be functionalized after synthesis. The introduction of functional groups can for instance be post-synthetic introduction of a functionalized linker [8] or introduction of metal nanoparticles [9]. This allows for specific engineering of functionalized MOFs with desired properties. Especially 3rd and 4th generation MOFs are investigated for the use in many applications.

1.2. Applications

MOFs are today studied for the use in many applications, for example in gas adsorption [10], catalysis [9], drug delivery [11] and electrochemistry [12]. The use of MOFs for gas adsorption will be discussed in the following section.

1.2.1. Gas adsorption

1.2.1.1. Carbon dioxide adsorption

The united nations framework convention on climate change (UNFCCC) agreed in Paris on the 12 of December 2015 on a new agreement to strengthen the global response on the increasing global temperature [13]. In order to reach this goal, a decrease in emission of greenhouse gases is needed. Capture and conversion of arguably the most famous greenhouse gas CO_2 is therefore a growing research field. MOFs are prime candidates for use as CO_2 capture materials.

In order to achieve a high adsorption capacity of CO_2, the pore volume of the MOFs is often functionalized. The introduced functional group needs to have a high affinity towards CO_2.

Some examples of interesting functional groups for this purpose are mentioned in the following paragraphs.

Incorporation of Lewis basic bipyridyl sites into UiO-67 was reported by Li et al. in 2013. This incorporation was achieved using the 2,2 – bipyridine-5,5´-dicarboxylate linker. The Lewis basic sites have a high affinity toward CO_2, CH_4 and H_2 and would have roughly the same surface area as UiO-67. At 77 K and 20 bars the H_2 uptake was 5,7 wt% (26,6 % higher than that of regular UiO-67). The CO_2 uptake at 293 K and 20 bars was 79,7 wt% and is comparable to the highest uptakes of CO_2 among MOFs [14].

Another research topic that have received a lot of attention in recent years are increasing the selectivity towards CO_2. Especially selective adsorption of CO_2 in a CO_2/CH_4 and CO_2/N_2 mixed atmosphere. Wang et al. showed that the selectivity towards CO_2 could be increased by the incorporation of functional groups that selectively binds CO_2. They did this by incorporating carbonyl and sulfone groups on the UiO-67 linkers. The results showed that both the functionalized UiO-67 MOFs had double the maximum uptake of CO_2 at 298 K and 1 atm. The selectivity for both the functionalized materials was 2-4 times higher than for UiO-67 [15].

1.2.1.2. Water adsorption

MOFs are investigated for the use as water adsorbents. Water adsorbents are desired for the use in dehumidification, thermal batteries and delivery of drinking water in remote areas. Yaghi et al published in 2014 an extensive study comparing water adsorption in Zr - MOFs and other porous materials. MOF – 805 was one of the tested zirconium MOFs for the use as adsorbent. MOF – 805 and 2,6-NDC MOF are similar and differ only by two hydroxyl groups on the linker. In order to compare the materials as water adsorbents, three criteria were designed. These criteria are listed below.

1) Pore filling or condensation of water into the pores of the solid must occur at low relative pressure (relative humidity) and exhibit a steep uptake behavior.

2) The material needs to have a high-water uptake capacity for maximum delivery of water and facilitate adsorption/desorption processes for energy efficiency.

3) The material must have a high cycling performance and be stable towards water.

In short, the results showed that a few Zr-MOFs did well in regards of the three criteria. In some of the experiments they performed better than some of the porous material in practical use today [16].

1.3. Construction of metal organic frameworks

MOFs are formed by connecting inorganic clusters using organic linkers. The structure of the clusters and linkers can vary. Four examples of different clusters are shown in figure 1.

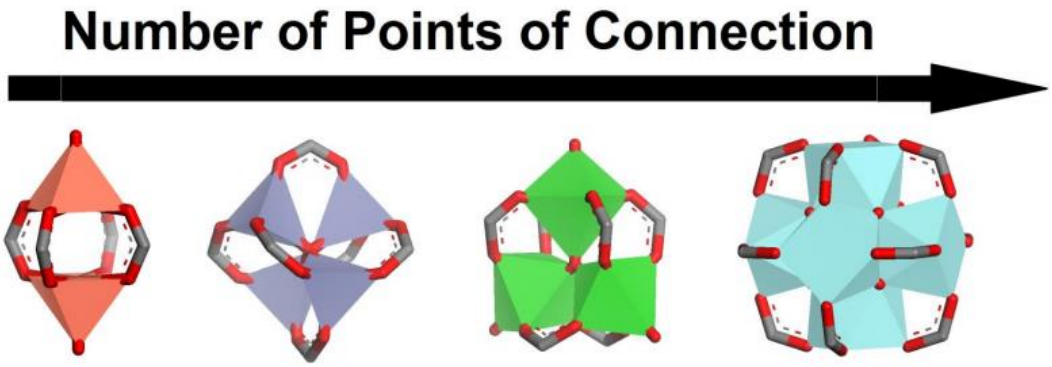

Figure 1: Four examples of inorganic clusters observed in MOFs. From left to right: paddlewheel cluster with the general formula $M_2L_2(CO_2)_4$, MOF – 5 cluster ($M_4O(CO_2)_6$), MIL – 101 cluster ($M_3OL_2X(CO_2)_6$) and UiO-66 cluster ($M_6O_4(OH)_4(CO_2)_{12}$) . M is a general metal cation, while L and X are neutral and singly negative charged ligands respectively [17].

The first cluster from the left is often referred to as the "paddlewheel" cluster which is adopted for Cu^{2+}- based MOFs such as HKUST-1 [18] with the general formula $\boldsymbol{M_2L_2(CO_2)_4}$, where M is a metal cation and L is a neutral ligand. The second cluster from left is the MOF – 5 cluster mentioned in section 1.1.2 and has the general formula $\boldsymbol{M_4O(CO_2)_6}$. The third cluster from the left, has the general formula $\boldsymbol{M_3OL_2X(CO_2)_6}$ and is the cluster of MIL-101 [19]. X is a singly negative charged ligand. The MIL - 101 and MOF - 5 cluster are both coordinated to six linker molecules but with different geometries. The fourth cluster from the left is the famous UiO zirconium cluster with the general formula $M_6O_4(OH)_4(CO_2)_{12}$. This cluster is often adopted by hard metal cations such as Zr^{4+} [3] and Hf^{4+} [20]. This is also the cluster of 2,6-NDC MOF and will be thoroughly explained in the following sections.

While many different inorganic clusters have been observed in MOFs, a much larger diversity are observed for the organic linker. In order to characterize a linker molecule, two terms are often used, geometry and topicity. The geometry of the linker refers to the angel between the groups that coordinates to the clusters [17]. The topicity refers to the number of functional groups that might connect to the cluster [21]. The focus in this thesis has been carboxylate-based linkers. Figure 2 illustrate a small selection of carboxylate linkers with different geometry and topicity.

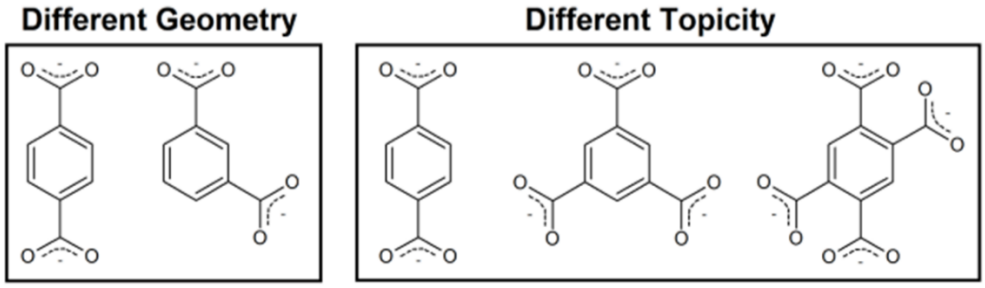

Figure 2: Left box, a selection of well-known linker molecules with different geometry. Right box, small selection of well-known linker molecules with different topicity [17].

1.3.1. The Zr_6 cluster

The superior stability of the Zr_6 clusters connected by dicarboxylate linkers can be rationalized using Pearson's hard/soft acid/base (HSAB) theory [22]. Zr^{4+} and CO_2^- are considered a hard acid and hard base respectively. Therefore, they are expected to form strong bonds.

The Zr_6 cluster will dehydroxylate if exposed to high temperatures according to the reaction equation below [23]. A temperature of 250 ℃ is enough to cause the cluster to undergo dehydroxylation. The reaction is reversible, and the clusters will undergo rehydroxylation if exposed to ambient condition.

$$\boldsymbol{Zr_6O_4(OH)_4 \overset{\Delta}{\Leftrightarrow} Zr_6O_6 + 2\,H_2O}$$

1.3.1.1. Crystal structure of a hydroxylated zirconium cluster

In a zirconium cluster there are six zirconium atoms. The zirconium atoms form an octahedron where each facet is capped by either an OH^- or O^{2-} group. The OH^- and O^{2-} are often denoted as $\mu_3 - O(H)$. Each zirconium atom is coordinated by eight oxygen atoms forming a square antiprism. Twelve linker molecules are connected to the zirconium cluster in the ideal structure. [2].

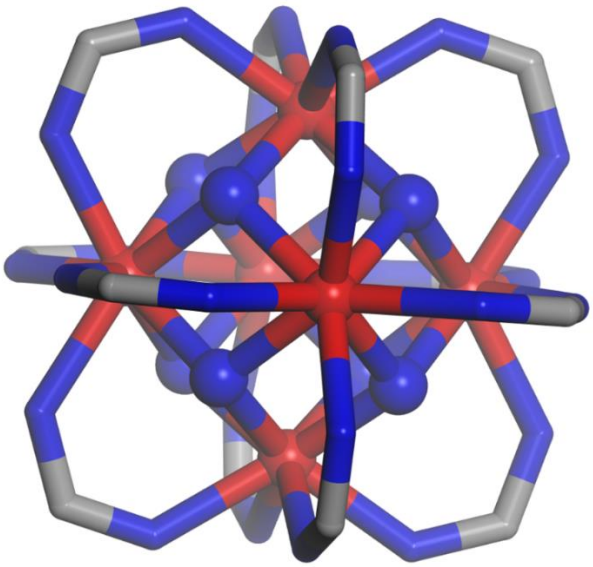

Figure 3: Illustration of a hydroxylated zirconium cluster. Oxygen, carbon and zirconium atoms are shown in blue, grey and red respectively. The core atoms of the zirconium cluster are shown by spheres. The carboxylate groups from the linker is illustrated as sticks. Hydrogens are omitted for clarity.

1.3.1.2. Crystal structure of dehydroxylated zirconium clusters

In a dehydroxylated zirconium cluster two water molecules have been removed. The coordination number of the zirconium atoms are reduced from eight to seven. The new coordination polyhedron around zirconium is a slightly distorted monocapped trigonal prismatic [24].

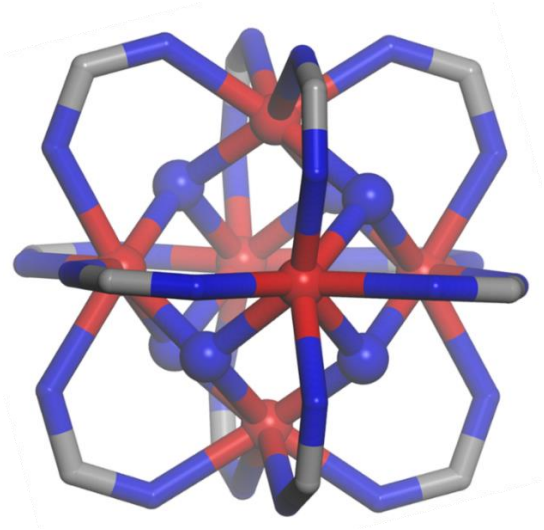

Figure 4: Dehydroxylated zirconium cluster. Oxygen, carbon and zirconium atoms are shown in blue, grey and red respectively. The core atoms of the zirconium cluster are shown by spheres. The carboxylate groups from the linker is illustrated as sticks. Hydrogens are omitted for clarity.

1.3.1.3. Reasoning for the high stability of the Zr_6 cluster

Pearson's hard/soft acid/base (HSAB) is qualitive concept. The theory suggest that hard acids form stronger bonds to hard bases, while soft acids form stronger bonds to soft bases. The properties of a hard/soft acid/base are described below.

1) A hard acid is characterized by a small ionic radii, high positive charge and high energy LUMOs
2) A soft acid is characterized by a large ionic radii, low positive charge and low energy LUMOs
3) A hard base is characterized by a small ionic radii, high negative charge and low energy HOMOs
4) A soft base is characterized by a large ionic radii, low negative charge and high energy HOMOs

The HSAB concept suggest that hard acids bonds strongly to hard bases because of a large columbic attraction. The bonding between a hard acid and a hard base is very ionic in nature. Soft acids bonds strongly to soft bases because of a large interaction between HOMO and LUMO. The bonding between a soft acid and a soft base is very covalent in nature [25].

1.3.2. 2,6-napthalene dicarboxylic acid

The 2,6-NDC linker is a carboxylate-based linker and is illustrated in figure 5.

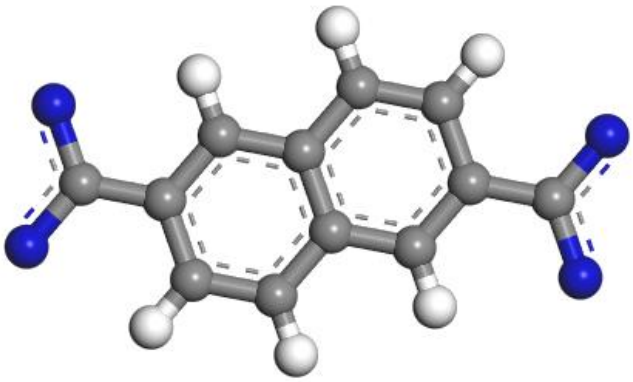

Figure 5: Illustration of the 2,6-napthalene dicarboxylate acid linker. Oxygen, carbon and hydrogen atoms are shown in blue, grey and white respectively.

A notable difference between the 2,6-NDC linker and the linker used in UiO-66 and UiO-67, 1,4 – benzendicarboxylic acid and biphenyl-4,4-dicarboxylic acid respectably, is the symmetry. While all the linkers contain some symmetry, the UiO-66 and UiO-67 linkers contain more symmetry elements, illustrated in figure 6.

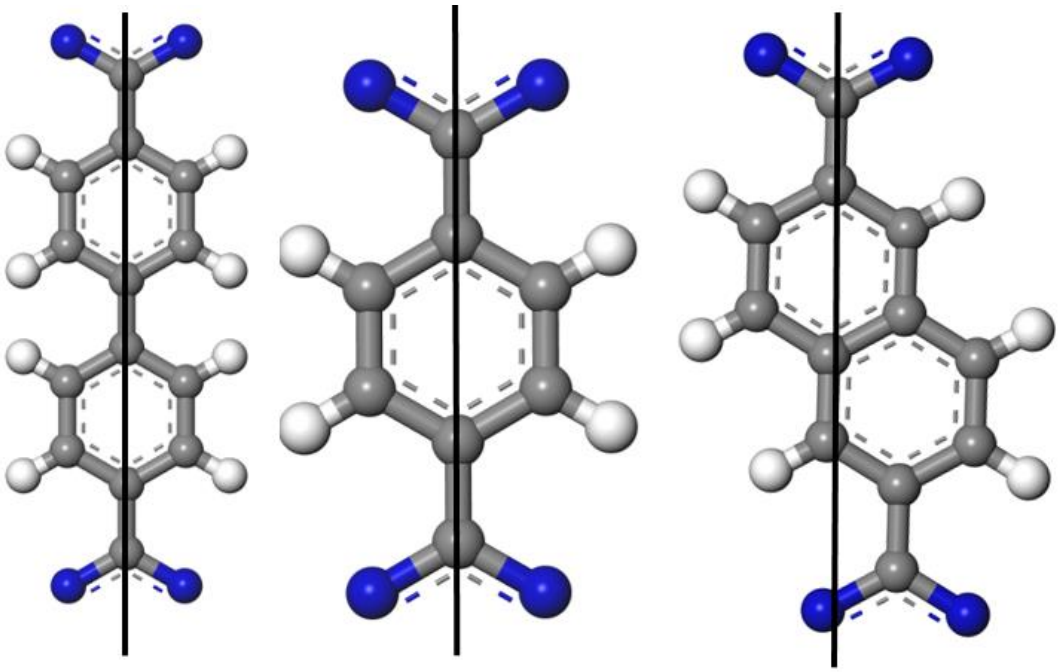

Figure 6: From left to right: The biphenyl-4,4-dicarboxylic acid (UiO-67 linker), 1,4 – benzendicarboxylic acid (UiO-66 linker)) and 2,6-napthalene dicarboxylate (2,6-NDC MOF linker). Black solid line: A mirror plane normal to the plane of the ring(s). Oxygen, carbon and hydrogen atoms are shown in blue, grey and white respectively.

From figure 6, its apparent that biphenyl-4,4-dicarboxylic acid and 1,4 – benzendicarboxylic acid contain a mirror plane perpendicular to the plane of the ring(s). The same mirror plane is not present in the 2,6-NDC linker. This has severe consequences for the symmetry of UiO-66, UiO-67 and 2,6-NDC MOF. UiO-66 and UiO-67 both belong to space group F m-3m (225) [26]. The F m-3m space group is a cubic space group with very high symmetry. The 2,6-NDC MOF will not obey the symmetry rules of the Fm-3m space group and must be described with triclinic symmetry. This is assuming that the structures do not have any atom position with an occupancy lower than one.

1.4. 2,6-NDC MOF

1.4.1. Connectivity of the 2,6-NDC MOF

The 2,6-NDC zirconium MOF was first synthesized and published in 2013 by kaskel et al. They reported a connectivity of twelve, eight and six for the 2,6-NDC MOF. The twelve connected framework is isoreticular to UiO-66 [27] and has been synthesized and characterized in this work. This MOF will be referred to as 2,6-NDC MOF. The 2,6-NDC MOF have a face centered cubic (FCC) structure. The chemical formula of 2,6-NDC MOF with hydroxylated zirconium clusters is $Zr_6O_4(OH)_4(C_{12}O_4H_6)_6$. A theoretical construction of the 2,6-NDC MOF is illustrated in figure 7.

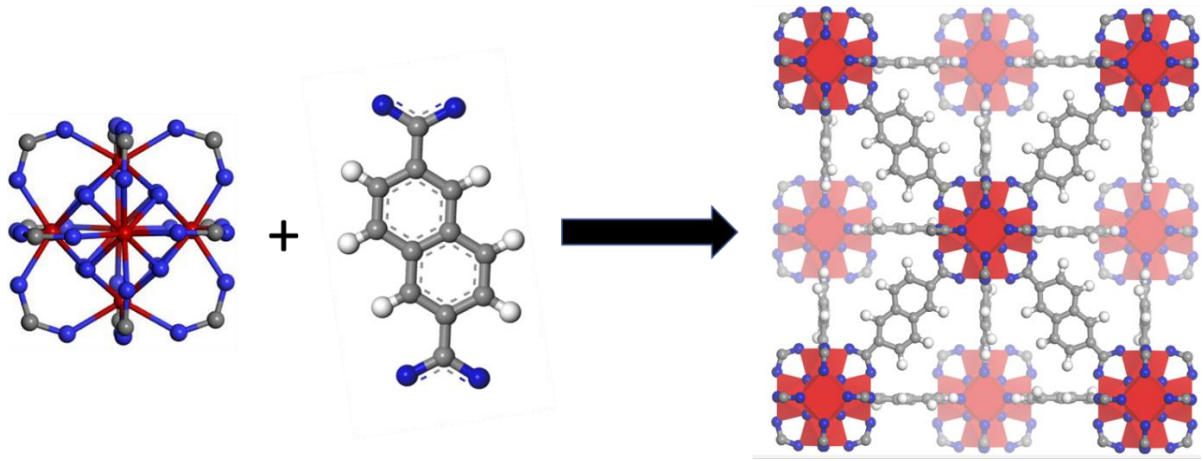

Figure 7: Theoretical construction of the 2,6-NDC MOF, showing how the linkers and clusters are coordinating to form a 3-dimentional framework. Oxygen, carbon, hydrogen and zirconium atoms are shown in blue, grey, white and red respectively. Zirconium coordination sphere is represented by a square antiprismatic polyhedron. Hydrogens on the clusters are omitted for clarity.

1.4.2. Structure of the cavities

There are two different pores in the 2,6-NDC MOF. These are different in size and shape. The pores are often referred to as the tetrahedral and the octahedral pores because of its resemblances to tetrahedral and octahedral holes in closest cubic packing.

1.4.2.1. The tetrahedral pores

In a tetrahedral pore, four clusters define the pore. A tetrahedral pore is illustrated in figure 8. As can be seen in figure 8, the hydrogen atoms on the linkers do not point towards the center of the pore but rather normal to the center of the cavity. This would make it hard for molecules in a tetrahedral hole to have an interaction with a potential functional group. Contrary to the hydrogen on the linker, the $\mu_3 - OH$ group on the zirconium cluster is pointing directly towards the center of the pore.

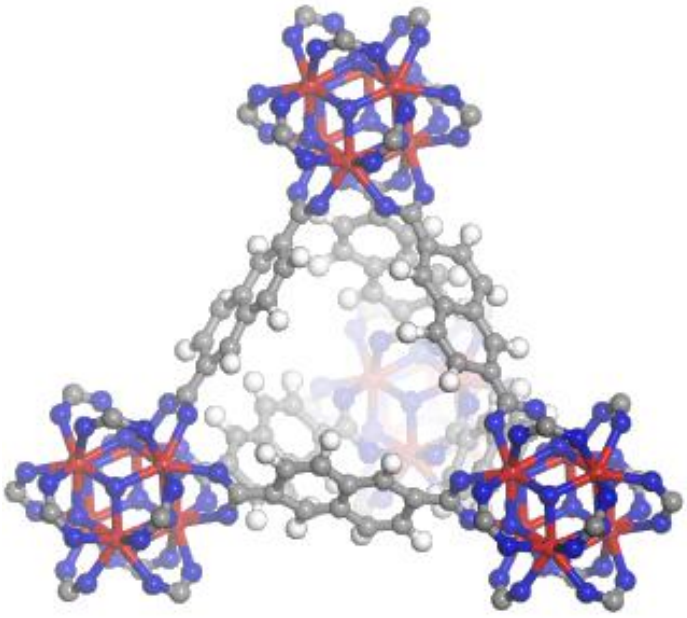

Figure 8: Tetrahedral hole for the 2,6-NDC MOF. Oxygen, carbon, hydrogen and zirconium atoms are shown in blue, grey, white and red respectively. Hydrogens on the clusters are omitted for clarity.

1.4.2.2. The octahedral pores

The octahedral pore is defined by six clusters. From figure 9 it is apparent that the hydrogens on the linkers points towards the pore. Molecules inside the octahedral pores can therefore have strong interaction with potential functional groups on the linkers. Contrary to the tetrahedral pores, the octahedral pores do not have any $\mu_3 - OH$ groups pointing towards the center of the cavity. The environment inside the tetrahedral and octahedral holes are therefore very different, both chemically and in size.

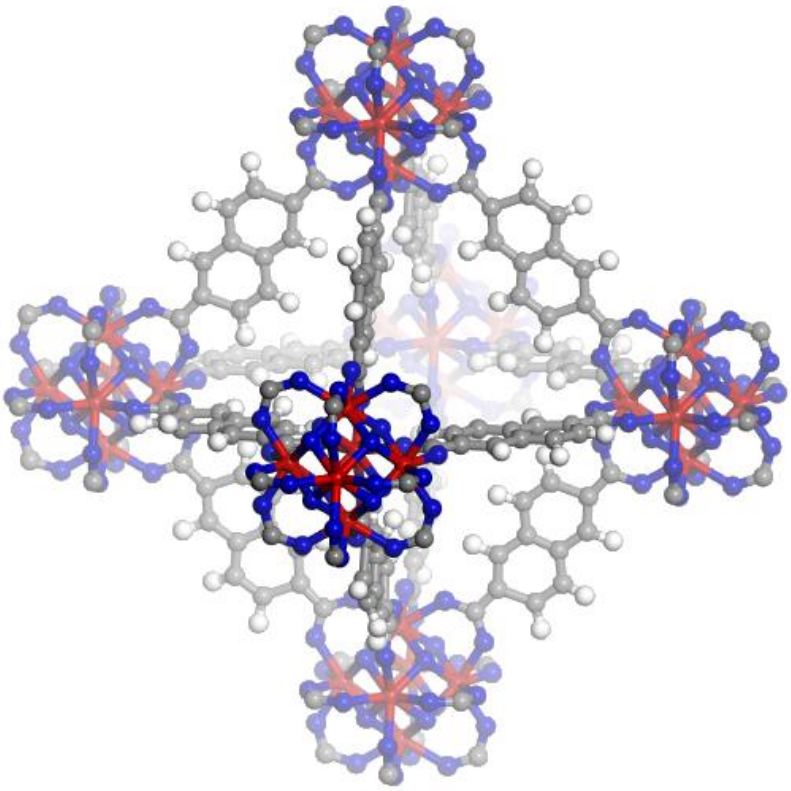

Figure 9: Octahedral hole for the 2,6-NDC MOF. Oxygen, carbon, hydrogen and zirconium atoms are shown in blue, grey, white and red respectively. Hydrogens on the clusters are omitted for clarity.

1.5. Functionalization of the 2,6-NDC linker

The arguably most interesting application of the 2,6-NDC linker is the vast possibilities of functional groups that can be incorporated on the linker. The chemistry of some functional groups will be greatly altered by the naphthalene linker.

1.5.1. 1,5-Dihydroxynaphthalene-2,6-dicarboxylic acid

1,5-dihydroxynaphthalene-2,6-dicarboxylic acid is a functionalized variant of the 2,6-NDC linker. This linker was used in MOF synthesis by Yaghi et al. and reported as MOF – 805 in 2014. MOF - 805 was used in the investigation of MOFs for water adsorption [16]. The linker is illustrated in figure 10.

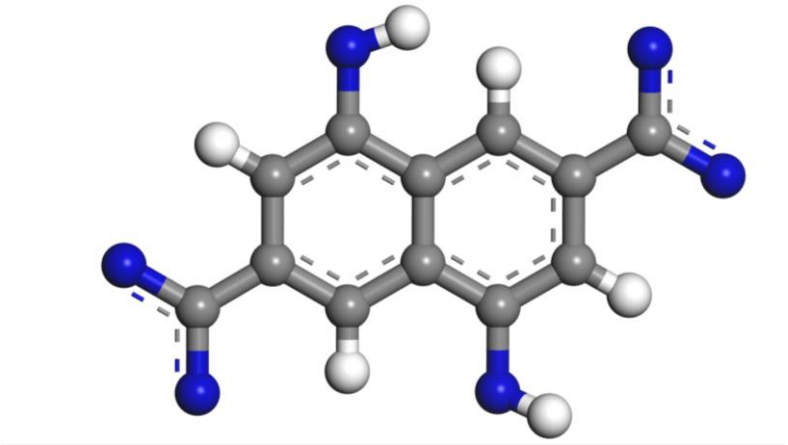

Figure 10: Illustration of the 1,5-dihydroxynaphthalene-2,6-dicarboxylic acid linker. Oxygen, carbon and hydrogen atoms are shown in blue, grey and white respectively.

1.5.2. 1,8-bis(dimethylamino) naphthalene-2,6-dicarboxylic acid

To date some of the most promising MOFs used in CO_2 capture are (alkyl)amine functionalized MOFs [28]. The 1,8-bis(dimethylamino)naphthalene molecule, often referred to as proton sponge, shows an unusually high basicity for an aromatic amine. Alder et al. proposed that the high basicity was attributed to steric strain in the neutral base which is effectively relived in the conjugated acid where a proton is intramolecularly hydrogen-bonded to the two nitrogen atoms [29].

An early ambition of this thesis was the purchase or synthesis of the 1,8-bis(dimethylamino) naphthalene-2,6-dicarboxylic acid. Unfortunately, no synthesis route or supplier was found for the functionalized linker. 1,8-bis(dimethylamino) naphthalene-2,6-dicarboxylic acid is shown in figure 11.

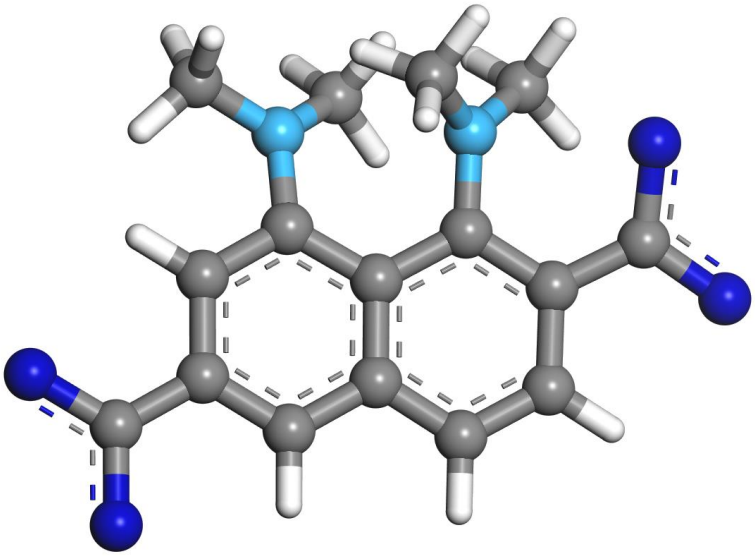

Figure 11: Illustration of 1,8-bis(dimethylamino) naphthalene with two acid groups. Oxygen, nitrogen carbon and hydrogen atoms are shown in blue, light blue, grey and white respectively. Hydrogen showed as sticks for simplicity.

1.6. Defects in 2,6-NDC MOF

Missing linker and missing cluster defects are the two main defects observed in 2,6-NDC MOF. Both types of defects have a large influence on the observed properties of the material. The effect of missing linker and missing cluster defects will be discussed in the following sections.

1.6.1. Missing linker defects

The chemical formula of the core atoms of a hydroxylated zirconium cluster is $Zr_6O_4(OH)_4$. The formal charge for each of the elements as well as the total charge of the cluster without ligands are listed in table 1.

Table 1: Overview of the formal charge of the elements in the Zr_6 cluster and the total charge of the cluster without charge balancing ligands.

Overview of formal charge to each atom in a zirconium cluster		
Element	**Formal charge**	**Total charge**
Zirconium	**IV**	**24**
Hydrogen	**I**	**4**
Oxygen	**-II**	**-16**
Charge sum for the cluster		**12**

From table 1 its apparent that twelve negative charges are needed in order achieve charge balance for the cluster. In an ideal 2,6-NDC MOF, twelve 2,6-NDC linkers are connected to the cluster. The 2,6-NDC MOF is said to contain missing linker defects when species other than the linker is connected to the cluster.

1.6.1.1. Background of missing linker defects

Missing linker defects in UiO MOFs were first described in 2013 by Zhou et al. They showed using high-resolution neutron power diffraction the first direct structural evidence of missing linker defects. They also investigated the composition of multiple batches of synthesized UiO-66 and concluded that the framework could accommodate a large variety of missing linker defects [10].

1.6.1.2. Effect of missing linker defects

The most important effects of missing linker defects are listed below:

1) MOFs with missing linker defects will contain other charge balancing ligands such as $-OH^-, -Cl^-$ and $-CH_3COO^-$ [17, 30]. Figure 12 illustrates how the structure changes when missing linker defects are introduced into the framework.

2) MOFs containing a large quantity monodentate ligands will have a lower thermal stability compared to the ideal MOF [30].

3) MOFs containing a large quantity of small monodentate ligands will have a higher specific surface area than the ideal MOF [10].

4) MOFs containing a large quantity of missing linker defects have been showed to have increased uptake of CO_2 at elevated pressures [10].

A MOF containing a large amount of monodentate ligands are expected to have a lower thermal stability. This is because a less connected material is formed when a large quantity of missing linker defects is present. A less connected material will have a lower thermal stability than the fully connected material.

It is expected that MOFs containing a large quantity of small monodentate ligands, will have a larger specific surface area. Small monodentate ligands are smaller than the large organic linker and therefore more free space inside the structure.

Zhou with co-workers published an extensive work on missing linker defects in UIO-66 and its effect on adsorption property. Their results showed that highly defective UiO-66 could accommodate more CO_2 than the less defective material. At one bar the defective material showed an 10 % increase in CO_2 adsorption. When this pressure was increased to 35 bars, an 50 % increase in CO_2 uptake was observed [10]. Missing linker defects can therefore be desired for certain adsorption purposes.

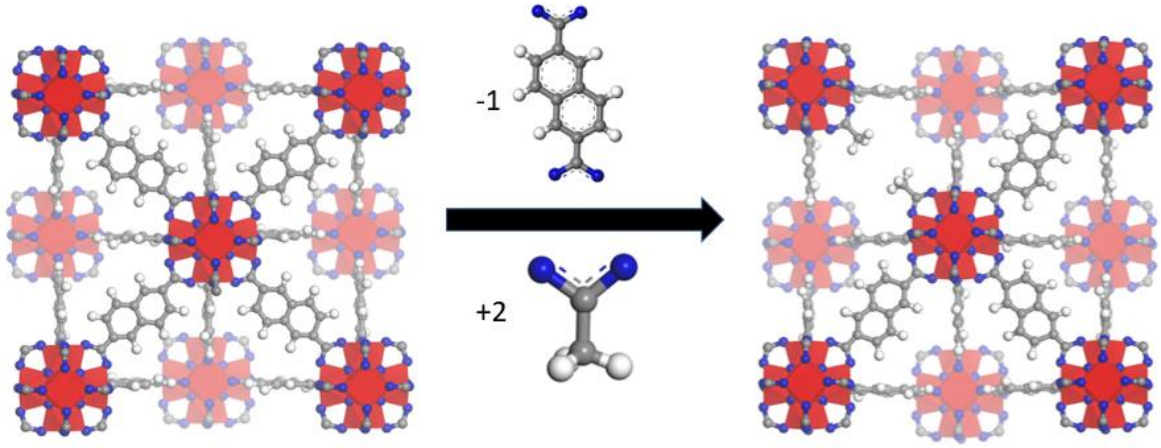

Figure 12: Theoretical replacement of a linker molecule for two acetate molecules. Oxygen, carbon, hydrogen and zirconium atoms are shown in blue, grey, white and red respectively. Zirconium coordination sphere is represented by a square antiprismatic polyhedron. Hydrogens on the clusters are omitted for clarity.

1.6.2. Missing clusters defects

Missing cluster defects are an important defect that can be observed in 2,6-NDC MOFs. When a cluster is missing in the framework, charge balance is required. Charge balance can be achieved by two possibilities. The remaining linkers can coordinate to another cation or monodentate ligands can replace the linker molecules. The latter is shown in figure 13 for acetate as the monodentate ligand.

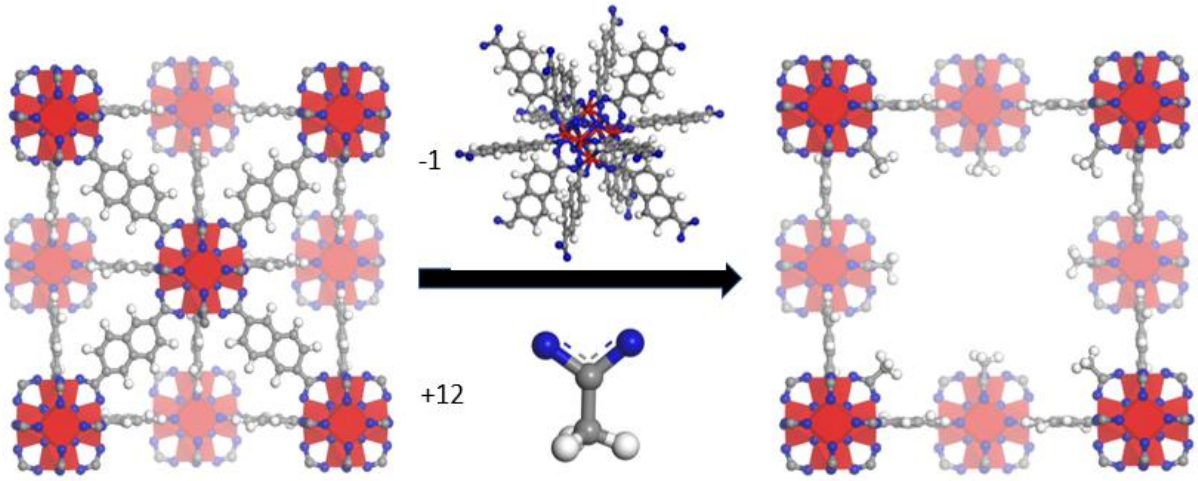

Figure 13: The removal of a cluster followed by the coordination of acetate ligands. Oxygen, carbon, hydrogen and zirconium atoms are shown in blue, grey, white and red respectively. Zirconium coordination sphere is represented by a square antiprismatic polyhedron. hydrogens on the clusters are omitted for clarity.

1.6.2.1. Background of missing cluster defects

Missing cluster defects were first thoroughly described by Goodwin et al in Nature Communication in 2014. A wide array of experimental characterization tools and computational techniques were applied in order to show that their experimental results could not be explained by solvent inclusion and/or missing linker molecules. This work was performed on UiO-66 with hafnium clusters [31].

1.6.2.2. Effect of missing cluster defects

Missing clusters defects alters some of the same properties as missing linker defects. The effects of missing clusters defects in the framework is listed below:

1) Missing cluster defects often leads to the incorporation of monodentate ligands such as $-OH^-, -Cl^-$ and $-CH_3COO^-$ [31].
2) MOFs containing a large quantity of missing cluster defects are expected to have lower thermal stability compared to the ideal MOF [30, 32].
3) MOFs containing a large quantity of missing cluster defects are expected to have a larger specific surface area compared to the ideal MOF [32].

Missing cluster defects alter the thermal stability and specific surface in the same manner as missing linker defects. The present of missing cluster defect results in a less connected material. Missing cluster defects also results in large empty pores which results in a larger surface area.

Koutsianos et al. published in 2019 a paper showing how cluster defects could be used for post-synthetic defects exchange (PSDE) of monodentate ligands. They used this technique to exchange acetate with other monodentate ligands with amino functionalities. This exchange was performed in attempts to increase the CO_2 uptake of the material. In the most successful attempt, almost 50 % increase in CO_2 uptake was measured [33].

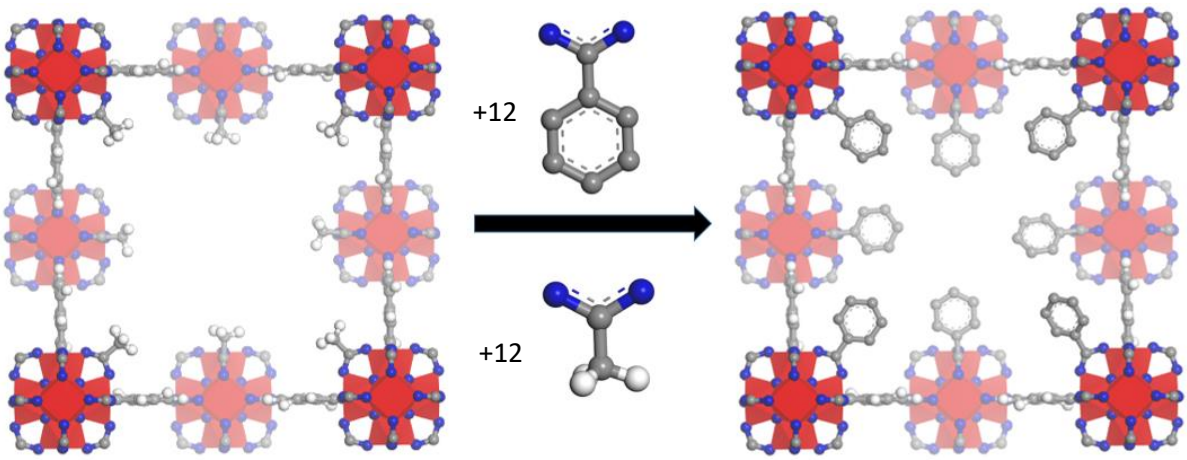

Figure 14: Illustration of how Koutsianos et al. proposed how a modulator (acetate in this case) could be replaced by a functionalized ligand. In this example a benzene ring is incorporated. Oxygen, carbon, hydrogen and zirconium atoms are shown in blue, grey, white and red respectively. Zirconium coordination polyhedron is represented by a square antiprismatic polyhedron. Hydrogens on the clusters are omitted for clarity.

1.7. Addition of modulator to the synthesis

The use of monocarboxylate species as additive in MOF synthesis have been shown to be important for size control of the crystallites and reproducibility of the synthesis. The first use of a modulator in Zr – MOF synthesis was applied in 2011 by Behrens et al. [34]. Since then the use of modulator have been extensively applied. The use of modulator can change the kinetics of the synthesis and the properties of the product.

In this thesis only monocarboxylate molecules have been used as modulators and is the only group of modulators that will be discussed. Some examples of monocarboxylate modulators are acetic acid, benzoic acid and formic acid. A modulator will compete with the linker during the synthesis. The modulator and linker bind reversibly to the metal cluster, but the linker will have a higher affinity towards the metal cluster. The incorporation of a modulator molecule will inhibit coordination sites and slow down the formation of nucleation sites. Increasing the concentration of the modulator further decreases the growth rate [21]. The use of modulator can therefore be used to synthesis larger crystals. Large crystals can be desired for many techniques such as structural elucidation using single crystal – XRD.

Another advantage of the addition of modulator to the synthesis, is the improved reproducibility. Behrens et al. reported that Zr - MOFs had much better reproducibility if benzoic acid was added to the synthesis. Without the addition of modulator, they reported that the previous procedure for Zr - MOF often resulted in an amorphous material [34].

2. Theory

2.1. Powder x-ray diffraction

2.1.1. Basic description of powder x-ray diffraction

A crystalline material has a three-dimensional long order at an atomic level. The smallest repeating unit is the unit cell. A unit cell is defined by the length a, b and c and the angles α, β and γ. The structure of the material is reproduced when the unit cell is repeated in three dimensions by translations. In a crystalline material, planes referred to as diffraction planes are present. These planes are identified by miller indices. Miller indices are a set of three numbers, h, k and l. Miller indices can be any integer from $-\infty$ and $+\infty$. A set of hkl values (for instance 111) will define a unique set of planes. The distance between these planes will be the interplanar spacing d_{hkl} [35].

X-ray diffraction (XRD) is arguably the most used characterization tool for crystalline materials. In an XRD measurement, monochromatic X – rays with known wavelength are directed towards the sample. The angle between the beam of X-rays, the sample and the detector are varied during the measurement. When the X-rays hit a diffraction plane at a certain angle constructive interference can occur. When constructive interference occurs, the signal is amplified. Constructive interference occurs when Braggs law is satisfied [36]. Braggs law is given in equation 1

$$\boldsymbol{n\lambda = 2dsin\theta} \qquad \textbf{(1)}$$

Where

$\boldsymbol{n}$ is an integer.

$\boldsymbol{\lambda}$ is the wavelength of the X-rays.

$\boldsymbol{d}$ is the interplanar spacing and.

$\boldsymbol{\theta}$ is the diffraction angle.

The angle at which constructive interference occurs is related to the interplanar spacing between the layers. XRD diffractograms can therefore act as a “fingerprint” for crystalline materials. If the sample is a powder, the technique is referred to as powder X-ray diffraction (pXRD),

In this thesis flat-plate sample holders have been used because of simple sample preparation and the small quantity of sample needed for a measurement. The biggest disadvantage of the flat-plate holders is that preferred orientation may occur. Preferred orientation occurs when the shape of the crystallites has a preferred orientation on the flat geometry. Plates and needles like crystallites are typical crystallites shapes that display preferred orientation. Cylindrical sample holders such as the glass capillaries can be used to almost completely remove preferred orientation. Capillaries sample holders can also be used for samples that are air sensitive [37, 38]

In order to produce X -rays with a known wavelength, a filament inside a cathode ray tube is heated. The filament will then start to produce electrons. These electrons are then accelerated towards a target material (often copper) by applying a voltage. If the electrons hit the target material with enough energy, core excitation of the target material can occur and X – rays with known wavelength will be formed. [36].

2.1.2. Usage in this thesis

The most important usage of pXRD have been for phase identification. In order to determine if the desired product had been synthesized a Rietveld refinement was performed.

By the comparison of the as synthesized pXRD pattern with the observed pXRD pattern after PSM, degradation could be detected. Lower signal to noise ratio, peak broadening and fewer peaks in the diffractogram are indications of degradation of the material.

PXRD patterns has also been used to identify missing cluster defects. Missing cluster defects alters the material to such an extent that it can be detected by pXRD. If the sample contains missing clusters defects small forbidden reflections in the pXRD diffractogram are observed.

The most frequent sample plate used during this thesis have been the glass plate for its simplicity. Full plate sample holders have been used when excess sample was available and higher quality pXRD data was required. A capillary pXRD sample holder have been used to remove preferred orientation of the isolated zirconium acetate clusters.

2.1.3. Experimental description

2.1.3.1. Glass plate pXRD

For a glass plate pXRD measurement, 30 mg of sample was added to the middle of the glass plate. In order to keep the sample on the plate, a plastic cover was used. The powder was then pushed flat using a micro slide. The intensity of the peaks in the pXRD pattern is sensitive to the quantity of sample. Therefore 30 mg of sample was used for each measurement. If the sample is not properly leveled incorrect peak positions, poor peak shapes and incorrect intensities may be observed [39].

A Bruker D8 Discover with a Lynxeye detector was used to obtain the pXRD results. A Ge (111) Johanssen monochromator was used to select Cu K-alpha – 1 radiation. The same instrument was used on full plate sample holders.

2.1.3.2. Full plate pXRD

A full plate pXRD measurement was performed by adding roughly150 mg of sample to the full plate. A micro slide was used to correctly level the sample.

2.1.3.3. Capillary pXRD

For a capillary measurement, a capillary with a diameter of 0,7 mm was packed with sample. The packed capillary was placed in a furnace at 100℃ overnight in order to activate the sample. The next day the capillary was sealed using a match.

In order to perform the measurement, the capillary had to be aligned. This was achieved by first installing the capillary to the top of the goniometer head using wax. The capillary was aligned before installing it in the instrument. The goniometer was adjusted in such a manner that the capillary was stationary when rotated 360°.

A Bruker D8 – A25 with a Lynxeye detector was used to obtain the capillary pXRD results. A Ge (111) Johanssen monochromator was used to select Cu K-alpha – 1 radiation.

2.2. Single Crystal XRD

2.2.1. Basic description of the technique

Single crystal – XRD was performed once in this thesis. A basic description of the technique is outside the scoop of this thesis.

2.2.2. Usage in this thesis

Single crystal XRD was used in this thesis for structural elucidation of the isolated zirconium acetate clusters. From a single crystal, the entire unit cell of the material was determined. Information such as bond lengths, coordination sphere and space group were derived from the unit cell.

2.2.3. Experimental description

The sample was first dispersed on a glass plate before the sample was investigated using an optical microscope. The optical microscope was used to find a single crystal of sufficient size. When a crystal large enough was found, the crystal was transferred to the sample holder. The sample holder was then installed into the instrument and aligned in such a way that the crystal was stationary while rotated around its own axis.

2.3. Thermogravimetric analysis and differential scanning calorimetry

2.3.1. Basic description of the technique

In a thermogravimetric analysis (TGA) measurement the weight of the sample is measured as a function of temperature in a controlled atmosphere. The change in the sample weight is caused by a chemical or physical process.

Differential scanning calorimetry (DSC) is a technique where the heat flow or power to the sample crucible and a reference crucible is monitored versus temperature. The instrument used in this thesis is a heat – flux DSC instrument. In a heat – flux DSC, the two crucibles are heated by the same heat source. The difference in temperature for the two crucibles must be the result of a physical or a chemical process in the sample crucible. This difference in temperature can be converted to a difference in power using a calorimetric sensitivity factor. This factor is different for each instrument [40]. The instrument used in this work can perform a TGA and a DSC measurement simultaneously.

Many factors are important when designing a TGA – DSC experiment such as choosing a crucible, atmosphere, temperature range and heating rate. The crucible must be chemical inert to the sample in the desired temperature range and in the specific atmosphere [41]. In some cases, a reaction between the sample and the atmosphere may be beneficial. An example of this is the reaction between zirconium and oxygen in the formation of ZrO_2 for zirconium MOFs.

2.3.2. Usage in this thesis

TGA – DSC measurements have been extensively used throughout this work because of its quick and easy sample preparation. TGA measurements can provide information regarding the physical and chemical processes occurring when the MOF is heated. Some of the most interesting processes are given below.

1: The desorption of solvent molecules from the pores of the MOF.

2: Dehydration of the zirconium clusters.

3: Loss of weakly-bonded species such as monodentate modulator.

4: Combustion of organic linker molecules.

It can often be hard to differentiate between process two and three because they take place in the same temperature range.

TGA can also be used to calculate the amount of missing linker defects. This will be discussed in detail in section 2.3.4.2.

DSC measurements was used to quantitatively determine the endothermicity or exothermicity of a process. DSC measurements were applied to provide important information about the thermal stability of the material under investigation.

2.3.3. Experimental description

The measurement starts with the instrument measuring the weight of the crucibles. Roughly 30 mg of sample was then added to a crucible. In order to get a reproducible sample surface, the sample was gently packed using a metal rod. The crucible was then placed on a loading dock for the instrument. Once the desired heating rate and atmosphere were chosen, the rest is automatically executed by the instrument. The temperature range was set to 30 to 800 ℃ using a heating rate of 5 ℃/min. The measurements were performed in synthetic air. The flow of oxygen and nitrogen was 5 ml/min and 20 ml/min respectively. Al_2O_3 was used as the crucible. TGA – DSC results were obtained simultaneously on a Netzsch STA 449 F3 – Jupiter instrument.

2.3.4. TGA analysis

2.3.4.1. Qualitative analysis of TGA results

A Typical TGA result for near defect free 2,6-NDC MOF is shown in figure 15.

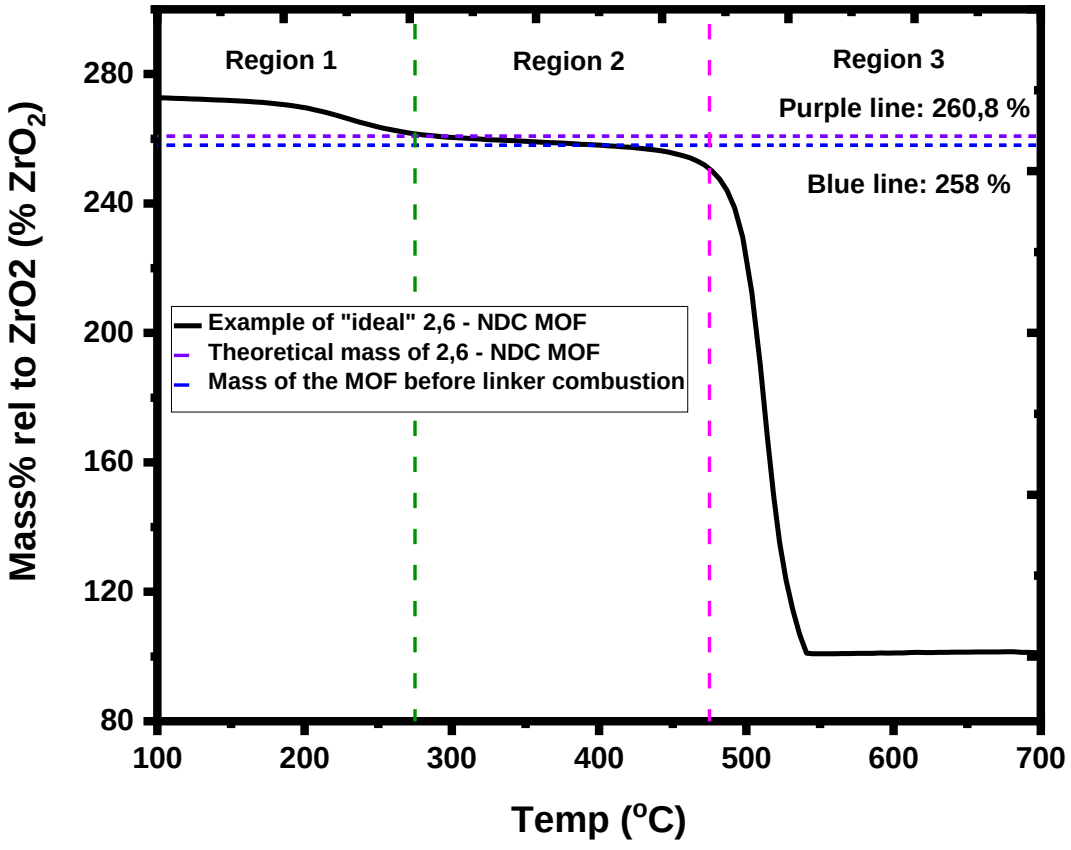

Figure 15: TGA results for near defect free 2,6-NDC MOF. Solid line: normalized TGA results. Horizontal dotted line: marks the theoretical (purple) and actual (blue) mass of the 2,6-NDC MOF. Vertical dotted lines: used to separate region 1,2 and 3 from each other.

In region 1 the mass loss is attributed to the evaporation of organic solvents and water adsorbed in the pores of the material during the synthesis. Two processes are believed to occur in region 2, both dehydration of the cluster and loss of weakly bonded species. Dehydration of the zirconium cluster is explained in section 1.3.1. The second process is believed to be the loss of weakly coordinated species such as acetate. The mass loss in the third region is attributed to the decomposition of the entire MOF structure resulting in the formation of zirconium oxide. The large mass loss observed in the third region will be discussed in the following section.

2.3.4.2. Quantitative analysis of TGA results

The chemical formula for ideal dehydroxylated 2,6-NDC MOF is $Zr_6O_6(C_{12}O_4H_6)_6$. The 2,6-NDC MOF is believed to decompose according to the following reaction equation:

$$Zr_6O_6(C_{12}O_4H_6)_6 + 72\ O_2 \rightarrow 6\ ZrO_2 + 72CO_2 + 18\ H_2O$$

The ratio of the molecular weight for ideal 2,6-NDC MOF and zirconium oxide can then be calculated using equation 2.

$$\frac{\boldsymbol{MW_{MOF}}}{\boldsymbol{6MW_{ZrO_2}}} = \boldsymbol{MW_{ratio\,\frac{MOF}{ZrO_2}}} \qquad \textbf{(2)}$$

Where:

$\boldsymbol{MW_{MOF}}$ is the molecular mass of the MOF.

$\boldsymbol{MW_{ZrO_2}}$ is the molecular mass of zirconium oxide.

$\boldsymbol{MW_{ratio\,\frac{MOF}{ZrO_2}}}$ is the molecular weight ratio of ideal 2,6-NDC MOF and zirconium oxide.

$$\boldsymbol{MW_{ratio\,\frac{MOF}{ZrO_2}} = \frac{1928\,\frac{g}{mol}}{6 * 123\,\frac{g}{mol}} = 2,61}$$

From the calculation its known that the molecular weight of ideal 2,6-NDC MOF is 2,61 times larger than the molecular weight of six formula units of zirconium oxide. The TGA results will be normalized and the weight of the zirconium oxide is set to 100%. The weight of the ideal 2,6-NDC MOF should therefore be 261 % before the combustion of the organic linkers. It is expected that the material contains missing linker defects if the weight is lower than 261 %. The chemical formula for a defective material is shown below. The chemical formula is only correct if the compensating ligand is monodentate.

$$\boldsymbol{Zr_6O_6(C_{12}O_4H_6)_{6-x}(compensating\ ligand)_{2x}}$$

TGA cannot be used to determine the identity of the compensating ligand. Therefore, a combination of other characterization techniques such as ls – NMR and EDX is applied. It should also be noted that the chemical formula above assumes there is only one compensating ligand. For simplicity the following discussing is limited to only acetate as the compensating ligand. Using this assumption, the new chemical formula for the 2,6-NDC MOF is shown below.

$$\boldsymbol{Zr_6O_6(C_{12}O_4H_6)_{6-x}(CH_3CO_2)_{2x}}$$

Equation 2 may be reorganized allowing for the calculation of $\boldsymbol{MW_{MOF}}$. The reorganized equation is shown in equation 3. The weight of the non-ideal MOF relative to the $\boldsymbol{6MW_{ZrO_2}}$ is shown in figure 16 and is $\boldsymbol{237}$%. This is below the theoretical value of $\boldsymbol{261}$%.

$$\boldsymbol{MW_{MOF} = MW_{ratio\frac{MOF}{ZrO_2}} * 6MW_{ZrO_2}} \quad \textbf{(3)}$$

As the molecular weight of ZrO_2 is known and $\boldsymbol{MW_{ratio\frac{MOF}{ZrO_2}}}$ was determined using TGA, the molecular weight of the defective MOF can be calculated using equation 3.

$$\boldsymbol{MW_{MOF} = 2,37 * 738\ \frac{g}{mol} = 1749\ \frac{g}{mol}}$$

The molecular weight of the material is $\mathbf{1749}\ \frac{\boldsymbol{g}}{\boldsymbol{mol}}$ which is substantial lower than $\mathbf{1927}\ \frac{\boldsymbol{g}}{\boldsymbol{mol}}$. The quantity of acetate can be calculated because the molecular weight of the linker, acetate and the cluster in a formula unit must add to the molecular weight of the MOF. As the molecular weight of the defective MOF have been established, the number of coordinated acetate molecules can be calculated using equation 4.

$$\boldsymbol{MW_{linker} * (6 - x) + MW_{Acetate} * 2x + MW_{cluster} = MW_{MOF}} \quad \textbf{(4)}$$

Where

$\boldsymbol{MW_{linker}}$ is the molecular weight of the linker.

$\boldsymbol{MW_{Acetate}}$ is the molecular weight of acetate.

$\boldsymbol{MW_{cluster}}$ is the molecular weight of the cluster.

$\boldsymbol{MW_{MOF}}$ is the molecular weight of MOF.

Equation 4 can be reorganized and solved for x

$$\boldsymbol{x = \frac{6MW_{linker} + MW_{cluster} - MW_{MOF}}{MW_{linker} - 2MW_{Acetate}}} \quad \textbf{(5)}$$

$$\boldsymbol{x = \frac{6 * 214 + 643 - 1749}{214 - 2 * 59,0} = 1,85}$$

In the chemical formula shown above, the quantity of acetate was 2x. Each cluster is accordingly coordinated to **3,7** acetate and **8,3** linker molecules in average. The correct molecular formula for this sample is given below.

$$\boldsymbol{Zr_6O_6(C_{12}O_4H_6)_{4,15}(CH_3CO_2)_{3,7}}$$

A similar analysis is inadequate when dealing with more than one variable. For instance, take a MOF where the compensating ligands are acetate, chloride and hydroxide. The new chemical formula is shown below.

$$Zr_6O_6(C_{12}O_4H_6)_{6-x-y-z}(CH_3CO_2^-)_{2x}(Cl^-)_{2y}(OH^-)_{2z}$$

This problem can be solved using the same method as above, but now there are multiple solutions for x, y and z. Additional information about x, y and z is needed in order to solve the equation. An example could be to find x using ^1H – NMR or y using EDX.

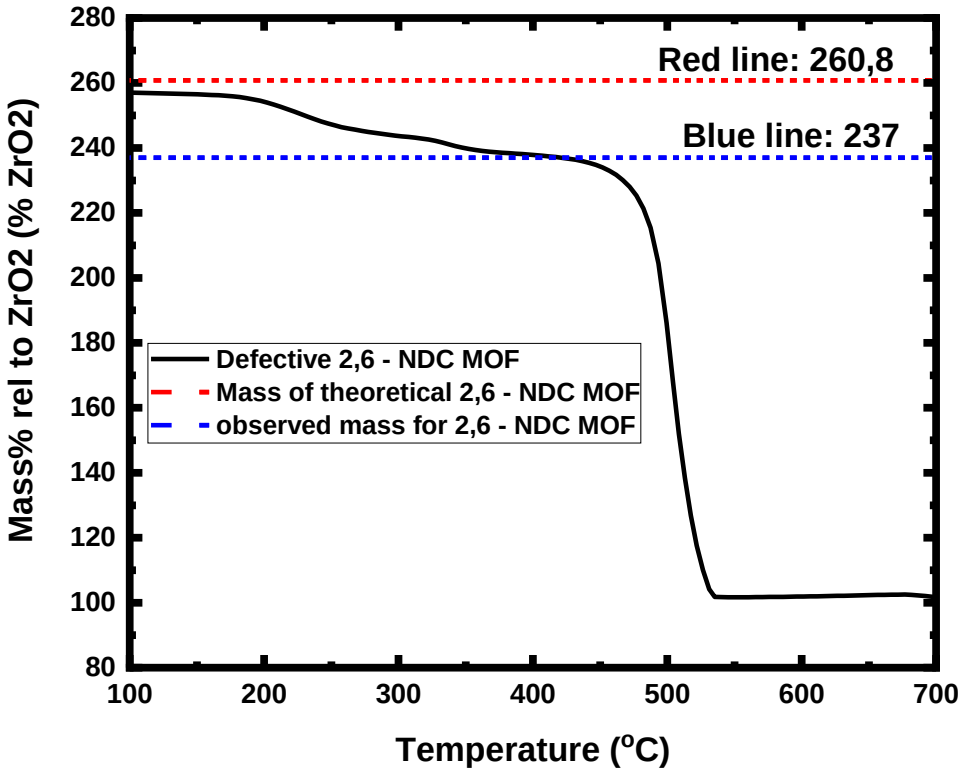

Figure 16: Normalized TGA results for defective 2,6-NDC MOF. Solid line: normalized TGA results. Dotted line marks the theoretical (red) and actual (blue) mass of the 2,6-NDC MOF.

2.4. Nitrogen adsorption

2.4.1. Basic description of the technique

Nitrogen adsorption measurements are a well known method used for determining the surface area of materials. This is achieved by first performing a nitrogen adsorption measurement and obtaining a nitrogen adsorption isotherm. Brunauer – Emmet – Teller (BET) theory can then be applied on the nitrogen isotherm in order to determine a specific surface area for the material.

There are three main methods for determining adsorptions isotherms, the volumetric, gravimetric and dynamic method [42]. In this thesis, a volumetric instrument was used. In a volumetric instrument a known volume of the adsorptive is dosed to the sample cell containing the adsorbent. The amount of adsorbate can be calculated from the pressure decrease in the adsorbent chamber.

There are many theories that can be applied for the analysis of a nitrogen adsorption isotherm. BET theory is the most widely applied theory for MOFs. BET theory is an extension of the Langmuir theory that allows for multilayer adsorption. It is based on many assumptions, the most important assumptions are shown below [43].

1: Each molecule adsorbed in a layer is a potential adsorption site for the next layer.

2: There is no steric limitation to the thickness of the multilayer.

3: The energy of adsorption for the first layer is equal and higher than the energy of adsorption for the succeeding layers which are also equal.

4: Interaction between molecules adsorbed in the same layer do not play any part in the adsorption equation.

Brunauer, Emmett and Teller was able to derive equation 6 based on these assumptions:

$$\frac{\boldsymbol{p_{rel}}}{\boldsymbol{V_m(1-P_{rel})}} = \frac{\mathbf{1}}{\boldsymbol{C * V_m}} + \frac{\boldsymbol{(c-1)}}{\boldsymbol{C * V_m}} * \boldsymbol{P_{rel}} \qquad \textbf{(6)}$$

Where:

$\boldsymbol{V_m}$: Volume of adsorbed nitrogen at monolayer capacity.

$\boldsymbol{p_{rel}}$: Relative pressure $(\frac{p}{p_0})$

$\boldsymbol{C}$: Is a constant related to the difference between the energy of adsorption for the first layer and the succeeding layers. $\boldsymbol{C \cong e^{\frac{Q1-Q2}{RT}}}$

By plotting $\frac{p_{rel}}{V_m(1-P_{rel})}$ against $\boldsymbol{p_{rel}}$, an approximately linear plot in the low pressure region is observed with the general formula of $\boldsymbol{Y = Slope * x + Constant.}$ Two new equations can then be derived.

$$\boldsymbol{Constant = \frac{1}{C * V_m}} \quad \textbf{(7)}$$

and

$$\boldsymbol{Slope = \frac{C-1}{C * V_M}} \quad \textbf{(8)}$$

This is an example of two equations with two unknowns and can be solved for C and V_M. Once V_M is known, equation 9 can be applied to calculate the BET surface area.

$$\boldsymbol{BET\ Surface\ area = \frac{n_a P V_M}{RT} * \sigma_0} \quad \textbf{(9)}$$

Where

$\boldsymbol{n_a}$ is Avogadro's number.

$\boldsymbol{P}$ is the atmospheric pressure.

$\boldsymbol{V_m}$ is the volume of the adsorbed nitrogen when the monolayer is formed

$\boldsymbol{R}$ is the universal gas constant.

$\boldsymbol{T}$ is the standard temperature.

$\boldsymbol{\sigma_0}$ is the cross sectional area of a nitrogen molecule.

A difficulty for the BET theory is the selection of an unambiguously $\boldsymbol{p_{rel}}$ interval for use in the BET analysis. One of the creators of BET theory, Brunauer, suggested that the analysis should be performed in the $\boldsymbol{p_{rel}} = 0.05 - 0.35$ Interval. In the case of microporous materials this interval is outside the linear region, and a smaller interval is required [43].

Another suggestion on how to choose an unambiguously $\boldsymbol{p_{rel}}$ interval, was the use of some simple criteria. These criteria are called the consistency criteria and were proposed by Rouquerol. There are in total four consistency criteria and they are listed below. For criteria three and four, a tolerance factor of **10** and **20%** was suggested respectively [43, 44].

1) Only a range where $\boldsymbol{N\left(1 - \frac{p}{p_0}\right)}$ increases as $\frac{\boldsymbol{p}}{\boldsymbol{p_0}}$ increase should be used in the analysis.
2) The value of C should be positive.
3) The monolayer loading, $\boldsymbol{V_m}$, should correspond to a relative pressure, $\frac{\boldsymbol{p}}{\boldsymbol{p_0}}$, within the pressure range used in the calculation.
4) The relative pressure corresponding to the monolayer loading should be equal to the relative pressure in criteria 3.

These consistency criteria are today widely used for the determination of a BET surface area. The purpose of the criteria was as mentioned to have a method of choosing an unambiguously $\boldsymbol{p_{rel}}$ interval for the analysis. The four criteria do limit the "allowed" $\boldsymbol{p_{rel}}$ interval for the analysis but is still far from an unambiguously $\boldsymbol{p_{rel}}$ interval.

2.4.2. Usage in this thesis

In this thesis nitrogen adsorption has been extensively used to measure the internal surface area of 2,6-NDC MOF, UiO-66 and UiO - 67. The ability to measure the surface area can be of great use as dramatic changes to the surface area are an indication of framework collapse. Nitrogen adsorption is therefore a possible technique for assessing if the framework is still intact after PSM.

The presence of missing linker and missing cluster defects also affect surface area of the material. For missing linker defects, the change in surface area is dependent on the size of the charge compensating ligand. If the charge compensating ligand(s) is smaller than the linker, the surface area is expected to increase with increasing defects. If the charge compensating ligand(s) is larger than the linker, the surface area is expected to decrease with increasing concentration of linker defects[32]. Missing cluster defects will generally results in a larger surface area [32]. Nitrogen adsorption measurements are therefore a tool used to check if a linker insertion was successful or if the sample contain missing cluster defects.

2.4.3. Experimental description

Three glass cells were evacuated and carefully weighted. Roughly 30 mg of sample was added to the cells. The cells were then mounted to the instrument and pretreated for one hour at 80 ℃ and then for two hours at 200 ℃ . The pretreatment was performed for the removal of organic solvents and water. The measurement was performed at −196 ℃. This was achieved by dispersing the class cells in liquid nitrogen. After the measurement was finished, the glass cells containing the pretreated material were weighted again.

All $\boldsymbol{p_{rel}}$ intervals used in a BET analysis was chosen to satisfy the consistency criteria if not stated otherwise. A tolerance factor of 10 and 20% was used for criteria 3 and 4 respectively. If more than one $\boldsymbol{p_{rel}}$ interval satisfied these criteria, the $\boldsymbol{p_{rel}}$ interval with the smallest tolerance factor in criteria four was chosen. A spreadsheet was used in order to evaluate all the possible solutions for the BET analysis. A minimum of five points on the nitrogen isotherm

was chosen for the BET analysis. With these additional criteria, an unambiguously $\boldsymbol{p_{rel}}$ interval was chosen.

Nitrogen adsorption isotherms were measured using a BelSorp mini II instrument.

2.5. Simulated nitrogen adsorption isotherms

Simulated nitrogen adsorption isotherms were obtained by the sorption tool in Material Studios. First the geometry of a nitrogen molecule was optimized using density functional theory in Material Studio. The quality of the optimization was medium and the local – density approximation functional was used. For the nitrogen isotherm simulation, the Metropolis Monte Carlo method was used. In this model the adsorbent is treated as a rigid structure and only rigid body translations and reorientations are incorporated [45]. The simulation was performed at -196 ℃. Each of the simulated adsorption isotherms had 51 points divided logarithmically, meaning that most of the measurement points were located at low pressures.

2.6. liquid state - nuclear magnetic resonance

2.6.1. Basic description of the technique

Liquid state nuclear magnetic resonance (ls-NMR) is a frequently used spectroscopy method in organic chemistry. Ls – NMR can be applied to any liquid containing atoms with spin. Atoms with an odd number of protons and neutrons will have a spin and will in the presence of a magnetic field orient itself relative to the field. For an atom with spin = 1/2, two different spin orientations exist, either parallel or anti parallel relative to the magnetic field. The orientation of the spin can flip from parallel to anti parallel if the atoms are exposed to electromagnetic radiation. The energy required for the atoms to flip orientation will be dependent on the identity of the atom and the strength of the magnetic field. The solvent and environment around the atoms will also affect the energy required to flip the orientation of the spin. The frequency that is required to flip the spin is called the resonance frequency. If the environment around two atoms are equal, the atoms are called equivalent. Two atoms with different neighbor atoms will have different resonance frequencies [46].

In a ls – NMR spectra the area under the peaks are proportional to the number of atoms responsible for the given peak.

A MOF must first be dissolved before ls-NMR can be applied. A dilute solution of NaOD is used as the 2,6-NDC MOF are not stable under basic conditions. Zirconium will react and precipitate as $Zr(OH)_4$. The linker, modulator and organic solvents will be deprotonated. Only the organic parts of the MOF are therefore suited for analysis using ls – NMR. In this thesis ^{1}H-NMR is primarily used.

An internal standard can be added to a ls-NMR experiment and produce quantitative results. It is important that the internal standard do not have any peaks overlapping with an analyte in the sample, this would result in interference. If no interference is present, the concentration of the analyte can be calculated with equation 10 [47]. An internal standard was not added in the ls-NMR result presented in this thesis.

$$C_{Analyte} = \frac{C_{standard}}{I_{Standard}} * I_{Analyte} * \frac{P_{Standard}}{P_{Analyte}} \quad \textbf{(10)}$$

Where:

$C_{Analyte}$: Concentration of the analyte

$C_{standard}$: Concentration of the standard

$I_{Standard}$: Integrated areal of the peak corresponding to the standard

$I_{Analyte}$: Integrated areal of the peak corresponding to the analyte

$P_{Standard}$: Number of spin active nucleus in the standard molecule

$P_{Analyte}$: Number of spin active nucleus in the analyte molecule.

2.6.2. Usage in this thesis

^{1}H-NMR has been extensively used in this thesis for the detection and identification of possible ligands such as acetate and formate. If a ligand was detected, the ratio $\frac{Linker}{Ligand}$ was calculated by the method described in section 2.6.3.

2.6.3. Qualitative analysis of ^{1}H-NMR results

By measuring the area under two or more peak, the ratio between the molecules corresponding to the peaks can be calculated. Topspin was used for the integration of the peaks. Figure 17 illustrate the liquid state ^{1}H-NMR results of a typical 2,6-NDC sample. The important peaks are marked with the corresponding Lewis structure of the molecule. Equivalent atoms are marked with the same number.

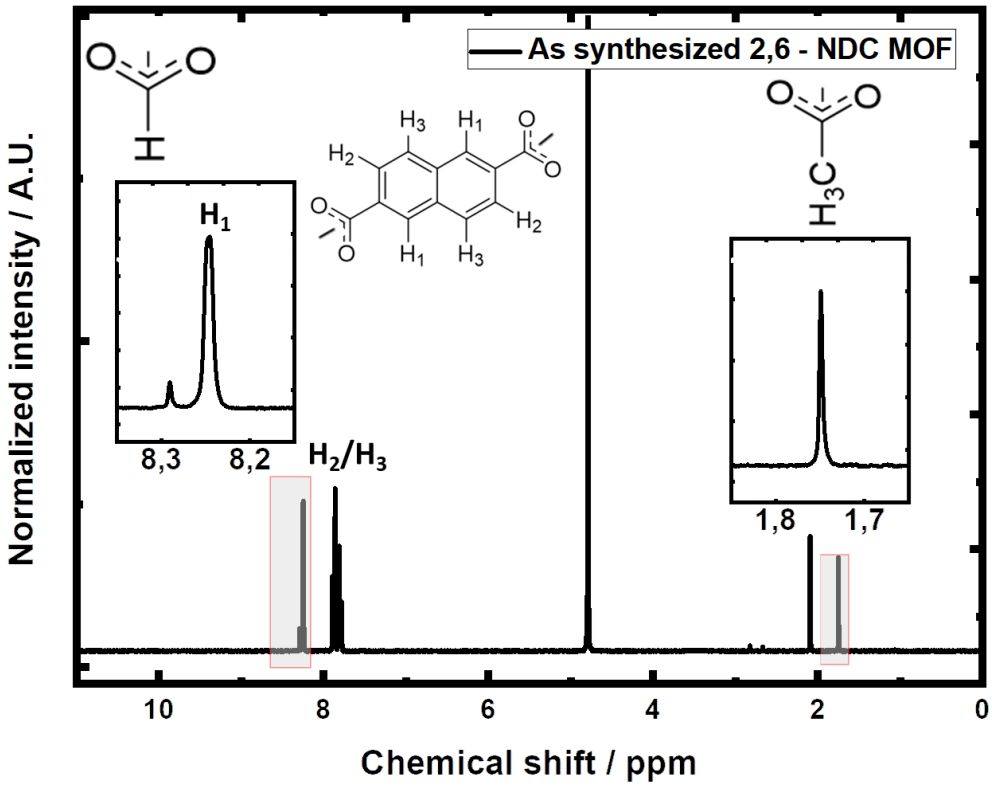

Figure 17: ^{1}H-NMR spectrum of a typical 2.6 – NDC MOF sample. The peak at 8,3 ppm is caused by formate and DMF. The peaks marked H_1/H_2 and H_3 correspond to hydrogens on the linker. The peak at 1,75 ppm correspond to acetate. The peaks at 4,8 and 2,1 ppm are water and dimethylamine respectively,

In this example the $\frac{linker}{Acetate}$ ratio will be calculated. The first step in the calculation is to choose which peaks that should be used for the integration. In figure 17 the peaks of interest are either marked or a Lewis structure is found on top of the peak. The peaks at 4,8 and 2,1 ppm are water and dimethylamine respectively. The peak at 8,25 ppm was chosen for the linker molecules and acetate only have one peak at 1,75 ppm. In table 2 the area of the linker peak is set to two. The area of the acetate peak is given relative to the areal of the linker peak.

Table 2: Linker to acetate ratio for the sample showed in figure 17. Integrated area for the linker is set to two. Area of the acetate peak is given relative to the area of the linker peak.

Sample	Area of the linker peak	Area of the acetate peak	Linker to acetate ratio
general 2,6 - NDC MOF	2	0,53	5,7

2.6.4. Experimental description

A 0,1 molar solution of NaOD was used to dissolve the 2,6-NDC MOF. The zirconium precipitates as $Zr(OH)_4$. The linker, modulator and organic solvents remains deprotonated in the solution.

A small spatula of sample was added to a centrifuge tube together with 0,8 mL of the dilute NaOD solution. The centrifuge tube was then mixed with the use of a mixer for ten minutes before it was centrifuged. 0,5 mL of this solution was then extracted by an automatic pipette and added to an NMR sample tube.

A Bruker AVIII HD instrument was used to obtain the ^{1}H – NMR results.

2.7. Scanning electron microscope

2.7.1. Basic description of the technique

In a scanning electron microscope (SEM), electrons are emitted from an electron source. These electrons are then accelerated towards holes in the anode plate. Electromagnetic lenses are used to control the path of the electrons. Normally the first lens is a condenser lens that focuses the electron beam. The condenser lens defines the size of the electron beam [48].

When the electron beam hits the sample, there are multiple of outcomes. The most important outcome for SEM is the backscattered electrons (BSE) and secondary electrons (SE). A BSE is the result of an elastic interaction with the sample while a SE is the result of an inelastic interaction. BSEs are detected by a solid state detector above the sample while SE are often detected by an Everhart-Thornley detector. The placement of the Everhart-Thornley detector is at the side of the sample.

A third outcome when the electron beam hits the sample is the formation of characteristic X-rays. When an electron with high energy from the electron beam hit the sample, some of its energy may transfer to the atoms of the sample. The electrons of that atom may use this energy to excite to a higher energy state or leaves the atom completely. When an electron falls back to a lower energy state, a photon with the energy equal to the energy difference of the two state is formed. The energy difference between the two states depends on the atomic number and is therefore a unique property of every element [49]. This is the working principle of energy dispersive X-ray spectroscopy (EDX).

2.7.2. Usage in this thesis

SEM was used in this thesis to investigate the topology of the synthesized material. The size of the particles was also investigated using SEM.

If copper tape was used in the mounting of the sample, EDX can be used to determine the elemental composition of the material. Chloride ions are for some MOFs a major source of defects and EDX was specifically used for the quantification of chloride [17].

2.7.3. Experimental description

A small patch of carbon tape was placed onto the sample holder. The sample was spread on top of the tape. Pressurized air was used to remove excess sample. The sample holder was then mounted in the scanning electron microscope.

SEM images were obtained using a Hitachi SU8230 Field Emission Scanning Electron Microscope.

3. Experimental

3.1. Reagent used in this work

$ZrOCl_2 * 8H_2O$ was used as the Zr – source in this thesis. $ZrOCl_2 * 8H_2O$ removed the need to add water to the synthesis. DMF was used as the solvent for the synthesis and acetic acid was used as a modulator. Ethanol was used in this work for the washing procedure of the material. The suppliers for the chemicals are listed below. All chemicals were used as purchased and no purification procedures were performed.

1) The 2,6-NDC linker was bought from Tokyo chemical industry (TCI).
2) $ZrOCl_2 * 8H_2O$ was bought from sigma Aldrich.
3) DMF was bought from ProfMOF.
4) 99 – 100% concentrated acetic acid was bought from VWR chemicals
5) Ethanol was bought from VWR.

3.2. Washing procedure

In this work two washing procedures were performed, filtration and centrifugation washing. The purpose of washing was to remove excess linker, modulator and ions such as chloride from the product. Filtration washing was performed if only a few samples needed to be washed. Centrifugation washing was applied if many samples were synthesized at once. This was because of the ease at which centrifugation washing could be applied to multiple samples at once.

3.2.1. Filtration washing

For filtration washing a filter membrane was placed on top of a filtering head. A filter cup was then put on top of the filter head and connected to the conical flask by a metal clamp. Before the filtration could start, the membrane had to be wetted, this was performed by filtering a few mL of DMF through the filter membrane.

The synthesis solution was poured into the filtering cup. If the synthesized material was stuck to the glass walls, sonication was used to disperse the material into the solution. A vacuum was created inside the conical flask, which forced the solvents through the filter membrane. The size of the holes in the membrane was either $2\ \mu m$ or $12 - 15\ \mu m$.

After the synthesis solution was filtrated, hot DMF was added to the filtration cup. After adding hot DMF, a glass rod was used to manually stir inside the filtration cup. The sample was left dispersed in the hot DMF for five minutes. After five minutes the sample was filtrated. This procedure was performed two more times but with ethanol instead of hot DMF.

3.2.2. Centrifugation washing

For centrifugation washing, the synthesis solution was simply poured into a glass vial of appropriate size. The vial was then centrifugated at 3000 rpm for roughly 5 minutes before the synthesis solution was decanted. The vial was then filled with hot DMF and the vial was shaken for 5 minutes. The sample was once again centrifugated at 3000 rpm for roughly 5 minutes before being decanted. This procedure was performed two more times but with ethanol instead of hot DMF.

3.2.3. Important details about the washing procedure

DMF and ethanol are both important in the washing procedure and are used for different purposes. Normally a $1:1$ molar ratio of zirconium and linker was used and therefore if no defects were present in the product, no excess linker should be present. As discussed, and shown in section 2.3.4.2., this is often not the case and linker defects are observed. The excess linker needs to be removed to obtain a single-phase sample. Therefore, one requirement of the solvent is that it solvates the linker molecules. In this work hot DMF was used to remove the excess linker molecules.

The use of ethanol in the washing procedure can be explained by a paper published by Fahra et al. Fahra and his group published a paper in 2014 investigating the stability of UiO MOFs. Their results showed that the removal of liquids with high surface tensions from the cavities of the MOF, causes strong capillary forces [50]. Ethanol is a relatively cheap solvent with a low surface tension ($22\ mN/m$) [51]. Other solvents such as acetone could also be applied with a minimal reduction in the surface area. If water is applied in the washing procedure and then evaporated from the cavities, the framework will collapse [51]. Water can therefore unfortunately not be used in the washing procedure.

3.3. Drying and storage

The washed product was transferred to a ceramic bowl and left in an oven for 24 hours at 120 ℃. After 24 hours, the product was transferred to a mortar and crushed gently with a pestle. The powder was then transferred using a funnel to a glass vial of appropriate size. The vials were sealed using plastic screw caps and kept in a plastic container.

3.4. Reaction equation for the formation of 2,6-NDC MOF

The reaction equation for the formation of 2,6-NDC MOF is shown below.

$$\mathbf{6}\ Zr^{4+}(DMF) + \mathbf{8}H_2O(DMF) + \mathbf{6}\ C_{12}H_6O_4^{2-}(DMF) \rightarrow\ Zr_6O_4(OH)_4(C_{12}H_6O_4)_6(s) + \mathbf{12}H^{+}(DMF)$$

3.5. Synthesis of 2,6-NDC MOF

3.5.1. Reflux procedure

2,9 g (300 eq) of DMF was added to an Erlenmeyer flask and mixed with 0,32 g (40 eq) of acetic acid. 0,043 g (1 eq) of $ZrOCl_2 * 8\,H_2O$ was transferred to the solution, before magnetic stirring and heating were applied. After reaching roughly 70 ℃, 0,029 g (1 eq) of 2,6-NDC was added to the Erlenmeyer flask. When the solution turned clear, the solution was transferred to a round bottle. The round bottle was placed in an oil bath at 120 ℃ for 24 hours under reflux with magnetic stirring. The samples were washed with the washing procedure described in section 3.2.1.

In the concentrated synthesis, only 100 molar equivalents of DMF and 20 molar equivalents of acetic acid was added to the synthesis. The procedure has been successfully scaled and applied to synthesis a few grams of 2,6-NDC MOF.

3.5.2. Autoclave procedure

The 2,6-NDC MOF has successfully been synthesized using a solvothermal method. The synthesize was performed using the same molar ratios as described in section 3.5.1.

All reactants were added to a Teflon lining. The Teflon lining was sealed inside an autoclave using four screws. The autoclave was then placed inside a furnace at 120 ℃ for 24 hours. After 24 hours the autoclave was cooled, and the product could be extracted and washed with the washing procedure described in section 3.2.1.

3.5.3. High throughput procedure

A high throughput procedure is a method in which many samples can be synthesized at once. This method was applied in the early stages of the thesis in order to screen different synthesis parameters.

In this work a metal plate with multiple holes, large enough to fit 6 mL vials were used. The metal plate was simply put on top of a heater and the entire plate was heated. An external thermostat was used in order to control the temperature. The molar ratios of the reactants changed for each vial, but the order of which they were added was the same as for the reflux procedure in section 3.5.1. The vials were left open during the reaction and the reaction time was 24 hours. The products were washed with the washing procedure described in section 3.3.2.

3.6. Synthesis of isolated zirconium acetate clusters

5 mL (100 eq) of water and 4,8 mL (30 eq) of acetic acid was added to a round bottle. 0,9 gram (1 eq) of $ZrOCl_2 * 8\,H_2O$ was then added to the solution of water and acetic acid. The round bottle was then put in an oil bath at 100 ℃ under reflux. After 24 hours the product was washed with the procedure described in section 3.2.1.

3.7. Post-synthetic ligand exchange

Post-synthetic ligand exchange (PSE) is a well-known PSM for decreasing the concentration of missing linker defects [52].

60 mL of DMF was added to a round bottle. 0,4g of 2,6-NDC MOF and 1 gram of linker were dispersed in the DMF. The round bottle was left under reflux in an oil bath at 120 ℃ for 24 hours. This procedure was also repeated without the use of a large excess of linker. The washing procedure described in section 3.2.1. was applied to wash the product.

The PSE procedure left the color of the solution and sample orange. The sample showed no degradation after the PSE procedure. After repeating the procedure without adding the MOF, the color was still observed. It seems that the MOF plays no part in the formation of the orange color.

3.8. Water stability

The 2,6-NDC MOF, UiO-66 and UiO - 67 were transferred to three ceramic crucibles each, resulting in a total of nine crucibles. All nine crucibles were placed under a large ceramic bowl turned upside down. A crucible filled with water was also placed under the large ceramic bowl. This was performed to expose the samples to an environment of high humidity.

After 24 hours a crucible containing 2,6-NDC MOF, one containing UiO-66 and one containing UiO-67 was activated in a furnace at 120℃ for 24 hours. After the sample was activated, a pXRD and a nitrogen adsorption measurement were performed to determine possible degradation of the material. These samples will be referred to as water activated.

The second set of samples were first dispersed in 6 mL of ethanol for 24 hours and then activated in a furnace at 120 ℃ for another 24 hours. Possible signs of degradation were investigated using a pXRD and a nitrogen adsorption measurement. These samples will be referred to as washed once.

The third set of samples were dispersed in 6 mL of ethanol for 24 hours and then decanted before once again being dispersed in ethanol for 24 hours. After being washed for the second time, the samples were activated in a furnace at 120 ℃ for 24 hours. Signs of degradation were determined using a pXRD and a nitrogen adsorption measurement. These samples will be referred to as washed twice. Table 3 summarizes the treatments performed on all the nine samples

Table 3: Summary of the sample names and treatments performed on the samples in the water stability experiment.

Sample	Treatment
UiO - 66 -, UiO - 67 - and 2,6 - NDC MOF-	Sample placed under high humidity and dried
Water activated	
UiO - 66 -, UiO - 67 - and 2,6 - NDC MOF-	Sample placed under high humidity, dispersed in ethanol for 24 hours before drying
Washed once	
UiO - 66 -, UiO - 67 - and 2,6 - NDC MOF-	Sample placed under high humidity, dispersed in ethanol for 24 hours twice, for a total of 48 hours before drying
Washed twice	

4. Results and discussion

4.1. Comparing experimental and simulated results.

4.1.1. Rietveld analysis

a pXRD diffractogram was calculated for the 2,6-NDC MOF using Material Studios. Material studios allows for direct comparison without the use of another software. The comparison is performed by a Rietveld refinement.

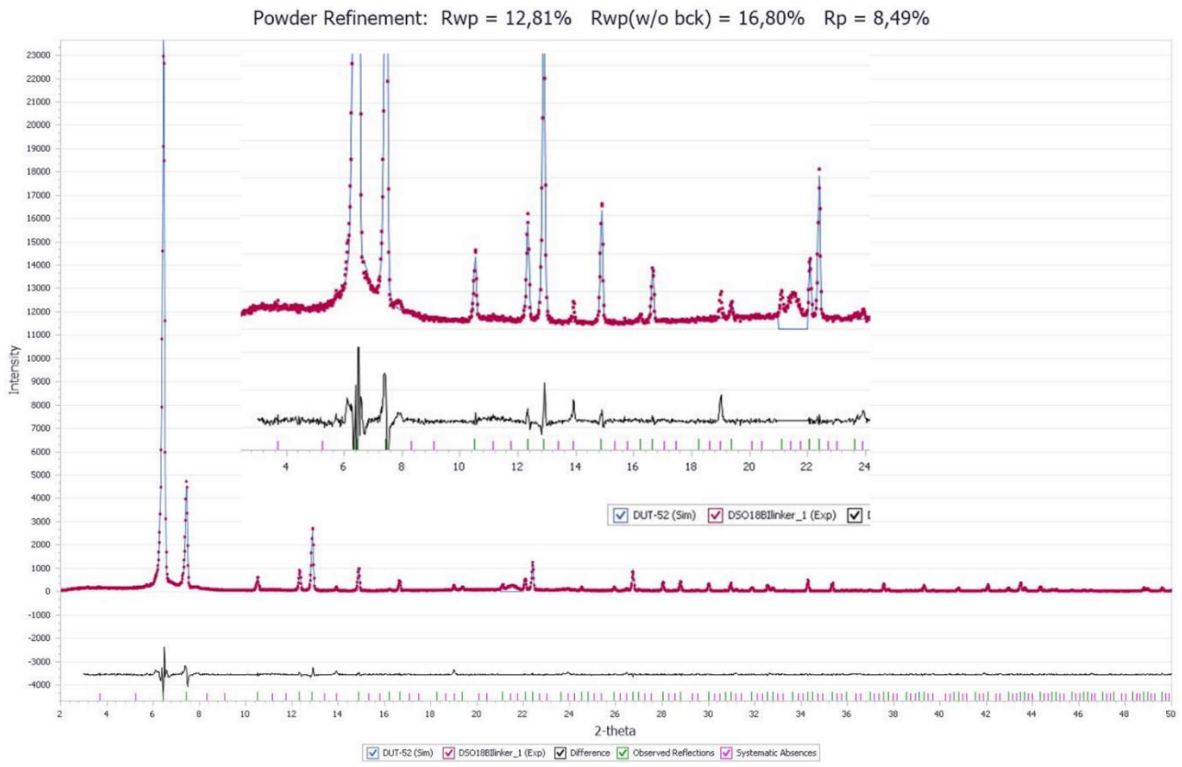

Figure 18: Rietveld refinement performed on 2,6-NDC MOF in Material Studios. The refinement parameters are included the top of the figure. Experimentally measured pXRD diffractogram is shown in red and the refined pXRD pattern is shown in blue. The black line shows the differential of the experimentally measured pXRD diffractogram and the refined diffractogram. The green and pink markers on the bottom of the figure show the allowed reflections in the Fm-3m and P1 space group respectively.

Figure 18 is an illustration of a Rietveld refinement performed in material studios. The corresponding R – values are listed at the top of the figure. The black line at the bottom is the difference of the experimentally determined diffractogram and the refined diffractogram. For a perfect fit, the black line should be straight. The large deviation from a straight line at low scattering angles is caused by the fact that the peak is asymmetric. The green and pink marks at the bottom of figure 18 illustrate the allowed reflections for the Fm-3m and P1 space group respectively. Some reflections observed for the 2,6-NDC MOF cannot be explained by the Fm-3m space group. For instance, the reflection observed at $2theta = 14$ is a forbidden reflection in space group Fm-3m but allowed for the space group P1.

4.1.2. Comparison of experimentally determined and simulated nitrogen adsorption isotherms

Comparisons of the experimentally measured and simulated nitrogen adsorption isotherms can give some insight in the synthesized material. Material Studios was used in order to simulate four nitrogen adsorption isotherms of different quality. The quality of the simulation increases in the following order: course, medium, fine and ultra-fine. The results are shown in figure 19.

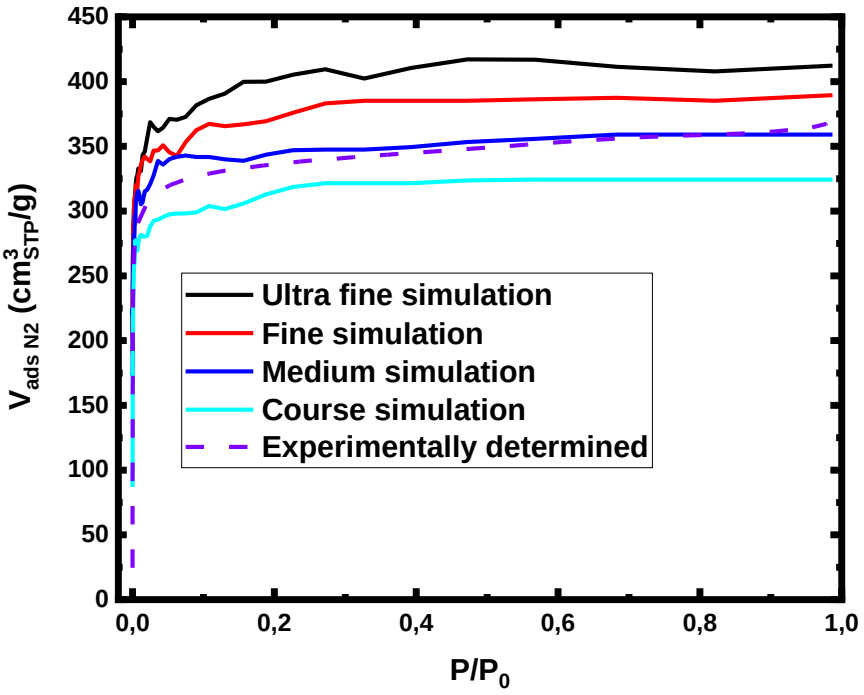

Figure 19: Comparison for the simulated and experimentally determined nitrogen isotherms obtained at -196℃. Solid line: simulated nitrogen adsorption isotherms. Dashed line: experimentally determined nitrogen adsorption isotherm.

Table 4: BET specific surface area for both the simulated and experimentally measured nitrogen adsorption isotherms shown in figure 19. The table summarize the specific surface areas and the pressure range used in the analysis.

BET analysis		
Sample:	**Pressure range (p/p_0)**	**Specific surface area (m^2g^{-1})**
Course simulation	0,0005 to 0,0032	1229
Medium simulation	0,0005 to 0,0032	1318
Fine simulation	0,0005 to 0,0032	1385
Ultra fine simulation	0,0005 to 0,0032	1393
Experimentally determined	0,0005 to 0,0036	1280

Criteria three and four were not fulfilled for the simulated isotherms. Criteria one is also disobeyed for the course, medium and fine simulation. This is an interesting difference between simulated and experimental determined isotherms. For low quality simulations, at very low relative pressures, the nitrogen uptake can decrease when the relative pressure increase. When this occurs, criteria one is disobeyed. This does not occur for an experimentally determined nitrogen adsorption isotherm.

It is apparent looking at the simulated isotherms in figure 19 that the maximum uptake of nitrogen (the plateau) increases as the quality of the simulation increases. For the BET analysis the same pressure range are used for all the isotherms. The BET surface areas are shown in table 4 and increases as the quality of the simulation increases. The BET surface area barely increases from a fine to ultra-fine simulation and may suggest that even better simulations might converge around $\mathbf{1400\ \frac{m^2}{g}}$**.** The discrepancy between the simulated and experimental determined values are discussed below.

Simulated adsorption isotherms are performed on ideal materials, which is never the case for experimentally determined isotherms. The cavities of the MOF may contain solvents or water if the pretreatment was insufficient. The presence of solvents or water will result in smaller measured surface area. Missing linker and cluster defects will also affect the surface area of the material as discussed in section 1.6.1.2 and 1.6.2.2 respectively.

The nitrogen adsorption isotherm simulation performed in Material Studios are of the Monte Carlo type. These simulations are not based on adsorption theory but uses random sampling to solve problems that might be deterministic [53]. It should therefore be used with caution.

4.1.3. The topology of 2,6-NDC MOF

A third tool that can be used to investigate the identity of the material is a SEM instrument. A SEM allows for the investigation of the topology of the sample. Crystallites of the 2,6-NDC MOF is shaped as octahedrons [27]. Ideal octahedrons have eight (111) facets [54]. Unstable facets will grow faster than stable facets. This indicates that the (111) facets for the 2,6-NDC MOF is relatively stable.

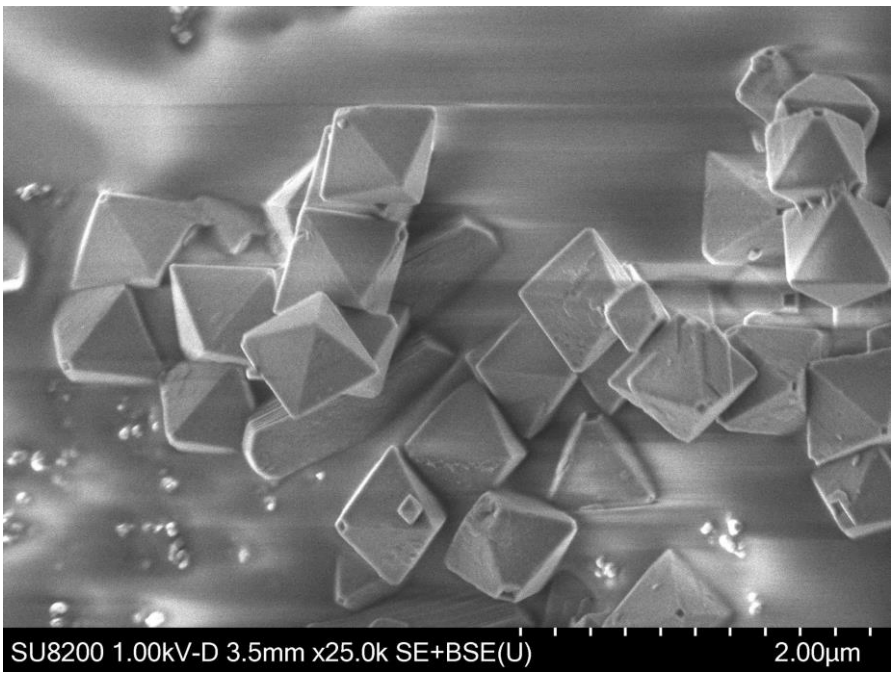

Figure 20: Scanning electron microscope image of 2,6-NDC MOF.

As can be seen in figure 20, the shape of the crystallites is clearly octahedra. Some of the octahedra are capped and some of them are fused together. The facet of the capped octahedra are (100). This is an indication that the (100) facets also grows relatively slowly. The size distribution of the particles varies but most of them are roughly $0{,}4\ \mu m$.

4.2. Missing Linker defects

Attempts to decrease the concentration of missing linker defects for the 2,6-NDC MOF will be discussed in this section. Many experiments were performed in order to investigate what parameter(s) affected the concentration of missing linker defect. The results of this investigation are summarized in the following sections.

4.2.1. Post-synthetic ligand exchange

Post-synthetic ligand exchange was one of the most successful methods applied to decrease the concentration of missing linker defects for the 2,6-NDC MOF. The experimental procedure for this technique is described in section 3.7. The TGA results are shown below.

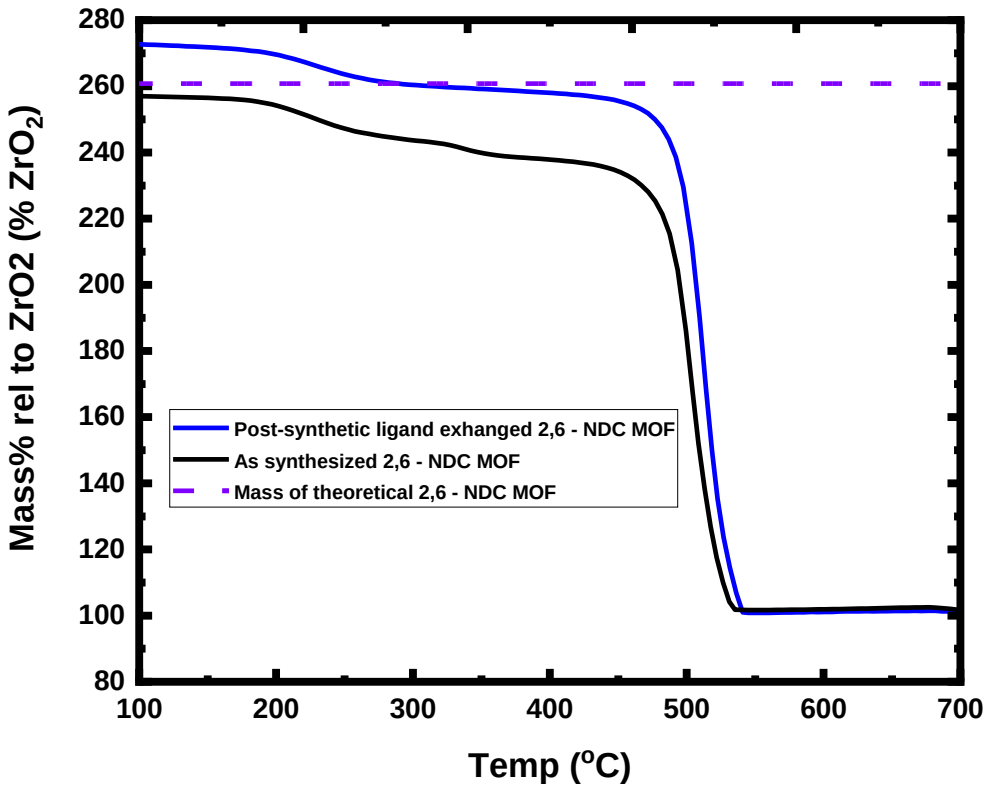

Figure 21: Solid line: normalized TGA results obtained before and after post-synthetic ligand exchanged. Dotted line: theoretical mass of dehydroxylated 2,6-NDC MOF.

As expected, the plateau for the post-synthetic modified 2,6-NDC MOF is higher than for the as synthesized material. This is because the other charge balancing ligands such as acetate have been exchanged by the linker during the PSE. The hypothesis that the PSE lead to a reduction in missing linker defects was investigated using ^{1}H - NMR. The ^{1}H-NMR spectra for both samples along with the as synthesized sample pretreated at 200℃ are depicted in figure 22. The linker to acetate ratios is summarized in table 5.

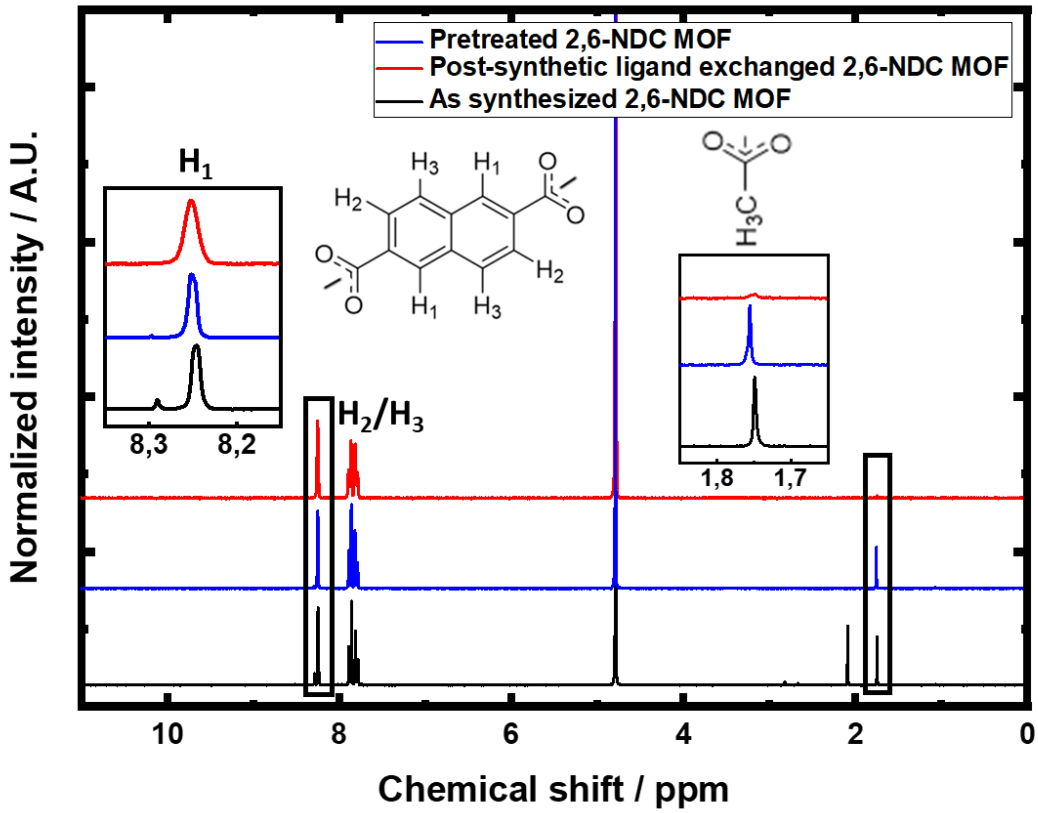

Figure 22: Normalized ^{1}H - NMR results obtained on the as synthesized, after pretreatment at 200℃ and after PSE samples. The peaks of great interest are indicated by the Lewis structure above to the peak. The peak at 2,1 ppm and 4,8 ppm are dimethylamine and water respectively.

Table 5: Linker to acetate ratio for the ^{1}H-NMR spectra showed in figure 22. Integrated area for the linker is set to two. Area of the acetate peak is given relative to the area of the linker peak.

Sample	area of the linker peak	Area of the acetate peak	Linker to acetate ratio
As synthesized 2,6-NDC MOF	2	0,53	5,7 : 1
Pretreated 2,6-NDC MOF	2	0,42	7,1: 1
Post-synthetic ligand exchanged 2,6-NDC MOF	2	0,06	50 : 1

For the as synthesized 2,6-NDC MOF the presence of DMF is confirmed by two peaks at roughly $2{,}9\ ppm$. These peaks are removed for the pretreated MOF. The DMF and formate peak overlap at $8{,}3\ ppm$, therefore a pretreatment of $200℃$ should be performed on the sample before attempting to quantify the amount of formate. A possible explanation for the increased linker to acetate ratio going from the as synthesized 2,6-NDC MOF sample to the pretreated 2,6-NDC MOF could be leftover acetate in the cavities of the material. From figure 22 it is apparent that dimethylamine is also removed from the cavities.

The formate and acetate peak are almost gone for the post-synthetic modified material suggesting that formate and acetate are exchanged by the linker. The exchange reaction of the linker with monodentate ligands is highly successful.

EDX was performed on reproduced samples. The results showed no indication of chloride in either the as synthesized sample or post-synthetic ligand exchanged sample.

In the above experiment, a large excess of linker was added in the PSE procedure. The waste of organic linker is undesired. In the following experiment the PSE procedure will be tested using different concentration of linker added to the procedure. First TGA was used to determine the quantity of missing linker defects of the mother material. The PSE procedure was then performed multiple times with different concentration of linker in the PSE. The quantity of added linker in the PSE procedure is shown in table 6. The quantity is given in % relative to the quantity of missing linker defects. For instance, DS037C is added the stochiometric amount of linker in order to form a defect free material.

Table 6: Summary of linker added in the PSE for each sample. The percentage is given relative to the calculated missing linker defects.

Linker added to the post modification	
Sample:	**Linker added**
DS037A	0 %
DS037B	50 %
DS037C	100 %
DS037D	150 %
DS037E	200 %

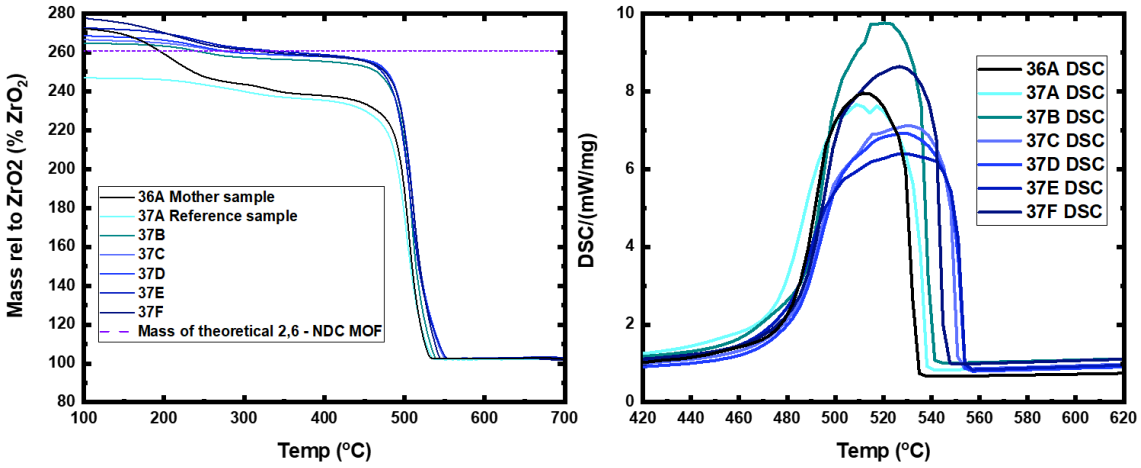

Figure 23: Left plot, solid lines: normalized TGA results obtained for the mother sample and after PSE. Dotted line: theoretical mass of dehydroxylated 2,6-NDC MOF. Right plot, DSC curves for the 2,6-NDC MOF samples before and after PSE.

DS037A is the reference sample, meaning that the sample has zero added linker in the PSE. Interestingly the TGA results indicate that the blank sample have a higher missing linker defect concentration than the mother sample. This is believed to be caused by the incorporation of formate originating from the hydrolysis of DMF. DMF can hydrolyze to formate and dimethylamine [55]. An exchange reaction between formate and linker may occur, causing a larger concentration of missing linker defects in the reference sample. This hypothesis could be tested by performing a ^{1}H-NMR experiment and calculating the linker to formate ratio. The linker to formate ratio would also decrease if another ligand was exchanged with the linker, however, no other known ligands were present during the PSE. Unfortunately, these samples were not pretreatment and therefore DMF may cause interference if the quantity of formate is determined using ^{1}H-NMR. If this hypothesis is correct, practical applications where exchange reactions may occur might be difficult.

Figure 23 also illustrate the ease of incorporating linker into the framework. Adding stoichiometric amount of linker results in an almost stoichiometric MOF. A large excess of linker is therefore not needed to obtain a material with few missing linker defects.

The DSC curves shown in figure 23 illustrate the improved thermal stability of the less defective materials. The thermal stability of the material might be defined by the temperature at which the DSC curve reached its maximum, sometimes referred to as the thermal midpoint. It is apparent from figure 23 that the thermal midpoints are at elevated temperatures for the less defective materials [56].

The thermal decomposition of MOFs is believed to start with breaking the binding between the metal cluster and the organic linker [57]. For a defective material there are significant fewer linkers connected to each metal cluster. A defective material is therefore less interconnected, and the decomposition is expected to occur faster for a defective material. A narrower DSC peak is expected for a defective MOF. This trend is observed in figure 23 except for DS037F. Its unknown why the DS037F sample do not follow this trend.

Post-synthetic ligand exchange has proven to be a superior procedure for decreasing the missing linker defects. PSE unfortunately do have a few drawbacks and some of them is listed below.

1) PSE leads to a large waste of linker. This is unfortunate because the linker can often be the most expansive part of the synthesis.
2) The PSE procedure requires the use of organic solvents for both the procedure as well as the washing procedure after. The usage of large quantities of organic solvents is expensive and have a negative effect on the climate.
3) The procedure of PSE adds additional work and time to the synthesis procedure for the ideal 2,6-NDC MOF.

4.2.2. Increasing the molar ratio of linker: zirconium

The effect of changing the molar ratio of linker to zirconium will be investigated in this section. It was hypothesized that adding a large surplus of linker will favor the incorporation of linkers. The samples were washed three times with hot DMF instead of one in order to remove excess linker. The molar ratios used in the synthesis are summarized in table 7.

Table 7: Overview of the molar ratios used in the synthesis.

$ZrOCl_2*8H_2O$: Linker: Acetic acid:DMF		
Under stoichiometric	Stoichiometric	Over stoichiometric
1:0,7:20:100	1:1:20:100	1:1,3:20:100

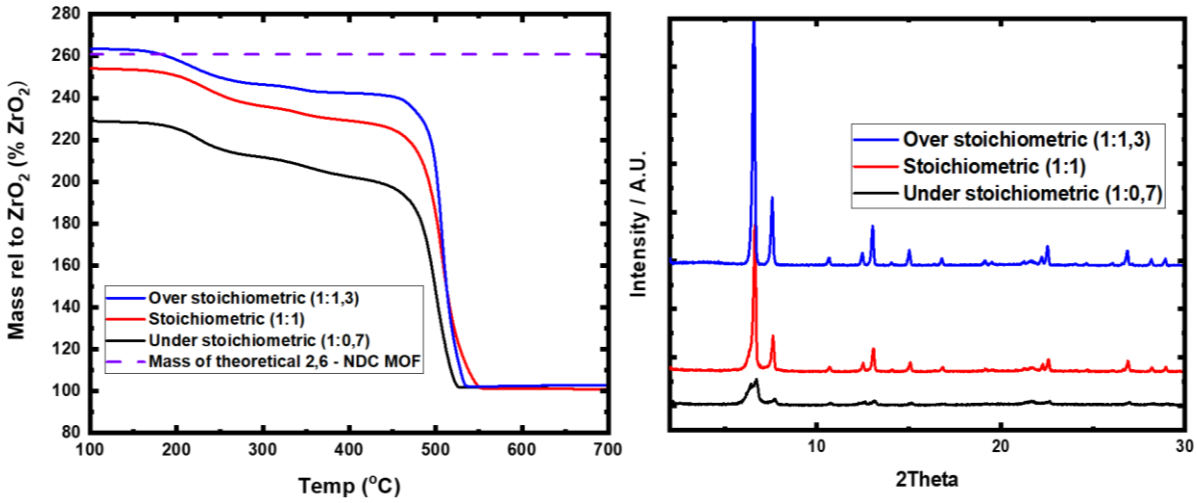

Figure 24: Left plot, solid lines: normalized TGA results for the three samples. Dotted line: theoretical mass of 2,6-NDC MOF. Right plot, pXRD results for the three samples. The samples were mounted with plastic film. The plastic film diffracts at 2theta = 20-22.

The under stoichiometric synthesis do not seem to form a crystalline material. Both the stoichiometric sample as well as the over stoichiometric sample seems to have formed the 2,6-NDC MOF. The TGA results indicate that the over stoichiometric sample contain fewer missing linker defects than the stoichiometric sample. The addition of excess linker in the synthesis seems to have pushed the equilibrium towards incorporation of linker.

4.2.3. Crystallization temperature

A very important parameter in MOF synthesis is the crystallization temperature. The crystallization temperature is reported in the literature to heavily effect the properties of UiO-66. The following mechanism was proposed by Greig Shearer.

1) The ligand exchange rate for Zr^{4+} is slow. Increasing the synthesis temperature is believed to lower the missing linker defects by increasing the rate at which the ligands exchange [17].

Based on this work for UiO-66, similar experiments were performed for 2,6-NDC MOF. The synthesis was performed at three different crystallization temperatures 100℃, 120℃ and 160℃. The samples were synthesized using the reflux method described in section 3.5.1. The results are shown below.

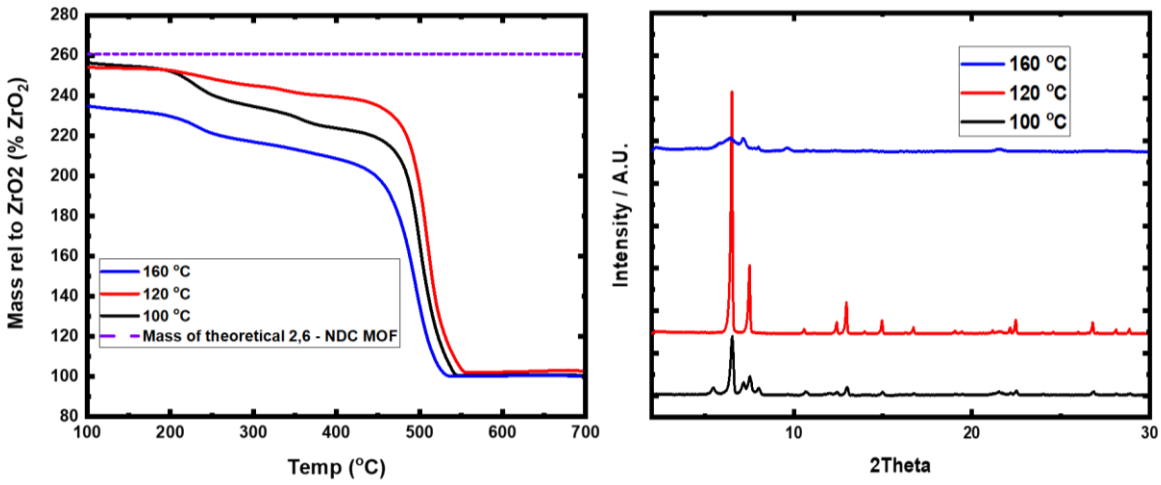

Figure 25: Left plot, solid lines: normalized TGA results for 2,6-NDC MOF with three different crystallization temperatures. Dotted line: theoretical mass of 2,6-NDC MOF. Right plot, pXRD results for 2,6-NDC with three different crystallization temperatures. The samples were mounted with plastic film. The plastic film diffracts at 2theta = 20-22.

The right plot of figure 25 shows the pXRD results performed on the three samples synthesized with a crystallization temperature of 100℃, 120℃ and 160 ℃. As expected, the pXRD result using a crystallization temperature of 120 ℃, is that of the 2,6-NDC MOF. The pXRD results obtained for the 100 ℃ shows extra peaks at roughly 2theta = 5,5, 7,2 and 8. The sample synthesized using a crystallization temperature of 160 ℃ seems to not be a crystalline material. The synthesis of 2,6-NDC MOF was therefore not successful at other crystallization temperatures than 120℃.

The left plot of figure 25 shows the TGA results for the three samples. The TGA results suggest that the least defective material was synthesized using a crystallization temperature of 120 ℃. The synthesis performed at 100 ℃ and 160 ℃ results in the second and third most defective material respectively.

4.2.4. Concentration of the synthesis with a high throughput method

It was shown by Gurpreet Kaur and co-workers that an important parameter for missing linker defects in UiO-67 is the concentration of DMF. In their work, the relationship between the molar ratio of DMF, zirconium and modulator were investigated. The results showed that samples synthesized using a solvothermal method with a small DMF to zirconium ratio, contained fewer missing linker defects [58]. A similar experiment was performed in this thesis for the 2,6-NDC MOF. Similar experiments performed by Kaur et al. is repeated using a high throughput method. The molar ratios used in the synthesis are shown in table 8 and the procedure is described in section 3.5.3.

Table 8: Overview of the molar ratios of each reactant added to each sample vial. The molar ratios of $ZrOCl_2 * 8H_2O$, linker, acetic acid and DMF are shown in black, red, green and blue respectively.

$ZrOCl_2*8H_2O$: Linker: Acetic acid:DMF			
A1	B1	C1	D1
1:1:0:300	1:1:0:100	1:1:0:50	1:1:0:35
A2	B2	C2	D2
1:1:20:300	1:1:20:100	1:1:20:50	1:1:20:35
A3	B3	C3	D3
1:1:40:300	1:1:40:100	1:1:40:50	1:1:40:35
A4	B4	C4	D4
1:1:60:300	1:1:60:100	1:1:60:50	1:1:60:35

After a visual inspection of the diffractograms as well as Rietveld refinements, the identity of the A3 and B2 samples were confirmed as 2,6-NDC MOF. Since both A3 and B2 produced the desired product, it is believed that the molar ratio of DMF to Acetic acid is important for the synthesis of 2,6-NDC MOF. The synthesis of a sample in-between A3 and B2 with the molar ratios of 1:1:25:150 will be discussed in section 4.3.3.

A closer inspection of the pXRD patterns for A3 and B2 exposed an interesting difference between them, illustrated in figure 26. A small and broad peak at $2theta = 3{,}2$ was observed for the B2. A similar peak at roughly $2theta = 4$ was observed by Greg Shearer for UiO-66. Greg Shearer concludes that this peak is an indication of missing cluster defects [32]. The observation of only one broad peak, suggest that the defective phase only exists in nanoregions [17]. The expected reflections for 2,6-NDC MOF with missing cluster defects are shown in figure 26. This unexpected result will be discussed in section 4.3.1.

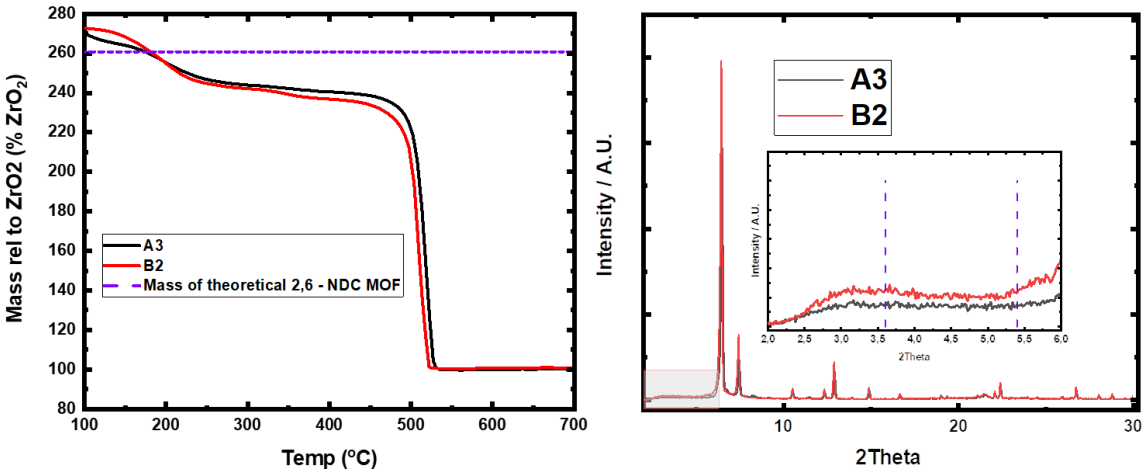

Figure 26: left plot, solid lines: normalized TGA results for A3 and B2 samples. Dotted line: theoretical mass of 2,6-NDC MOF. Right plot, pXRD results for the A3 and B2 samples. Vertical dotted lines illustrate the expected reflections for 2,6-NDC MOF with missing cluster defects. The samples were mounted with plastic film. The plastic film diffracts at 2theta = 20-22.

The TGA results are very similar for the two samples, with the A3 having fewer missing linker defects. The difference in missing linker defects for the two samples are very small and probably not significant if the procedure was repeated and statistical tools were applied. Concentrating the synthesis in autoclaves was attempted in order to reproduce Gurpreet Kaur et al. results. The results are described in the following section.

4.2.5. Concentration of the solvothermal synthesis

Synthesis of the A3 and B2 samples described in section 4.2.4. was performed in autoclaves. The A3 and B2 samples reproduced in autoclaves will be referred to as dilute and concentrated samples respectively. This experiment was performed in order to reproduce the results obtained by Kaur with co-workers, described in section 4.2.4. TGA and pXRD results for the experiment are shown in figure 27.

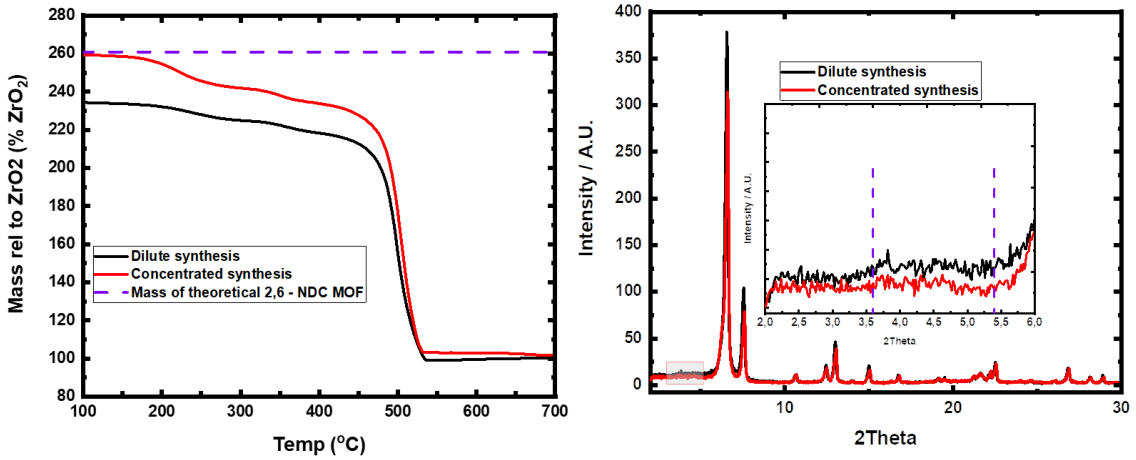

Figure 27: left plot, solid lines: normalized TGA results for dilute and concentrated samples. Dotted line: theoretical mass of 2,6-NDC MOF. Right plot, pXRD result for dilute and concentrated samples. Vertical dotted lines: illustrate the expected reflections for 2,6-NDC MOF with missing cluster defects. The samples were mounted with plastic film. The plastic film diffracts at 2theta = 20-22.

The diffraction peak at $2theta = 3{,}2$ are not observed for the concentrated sample. This result will be discussed in section 4.3.2.

The TGA results suggest that the dilute synthesis sample contain a significant fewer missing linker defects than the concentrated synthesis. This result agrees with the observed results for Kaur et al. However, both the materials contain a large quantity of missing linker defects.

4.3. Missing cluster defects

4.3.1. Concentration of the synthesis with a high throughput method

The pXRD results illustrated in figure 26 indicated that the B2 sample contained missing cluster defects. A nitrogen adsorption measurement was performed in order to check this hypothesis. If the hypothesis is correct, the B2 sample should have a higher specific surface area than A3.

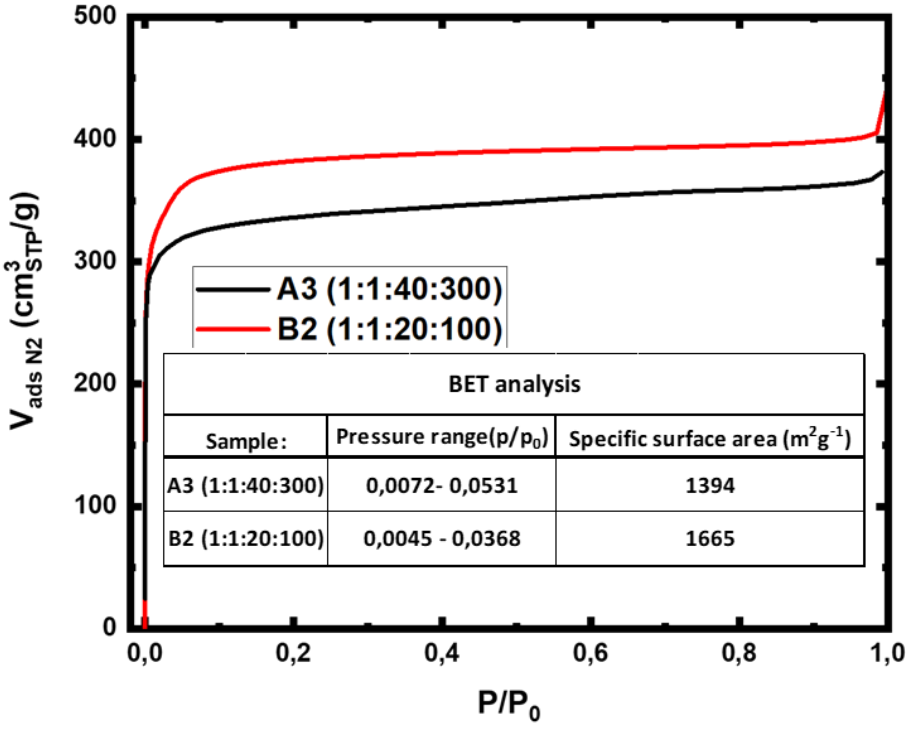

Figure 28: Comparison of the nitrogen adsorption isotherms for B2 and A3 samples obtained at −196 ℃. Table: specific BET surface area for both the A3 and B2 samples.

The nitrogen adsorption isotherm as well as the specific BET calculated surface area suggest that missing cluster defects are present in the B2 sample. Other reasons for the large difference in surface areas could be that the cavities of the A2 sample is filled by solvents. Both the A3 and B2 samples received the same washing procedure and the same pretreatment before the measurement. The cavities should contain the same amount of impurities. As already mentioned, the TGA results in figure 26 suggest the samples have roughly the same amount of missing linker defects. The difference in BET specific surface area can therefore not be explained by missing linker defects. It was concluded based on the pXRD results and the nitrogen adsorption isotherms that missing cluster defects were present in the B2 sample.

4.3.2. Concentration of the solvothermal synthesis

From the pXRD diffractogram illustrated in figure 27, it was not expected that the concentrated synthesis contains missing cluster defects. The TGA results in figure 27 showed that the concentrated synthesis contained fewer missing linker defects. It is therefore expected that the sample with the highest surface area is the dilute sample.

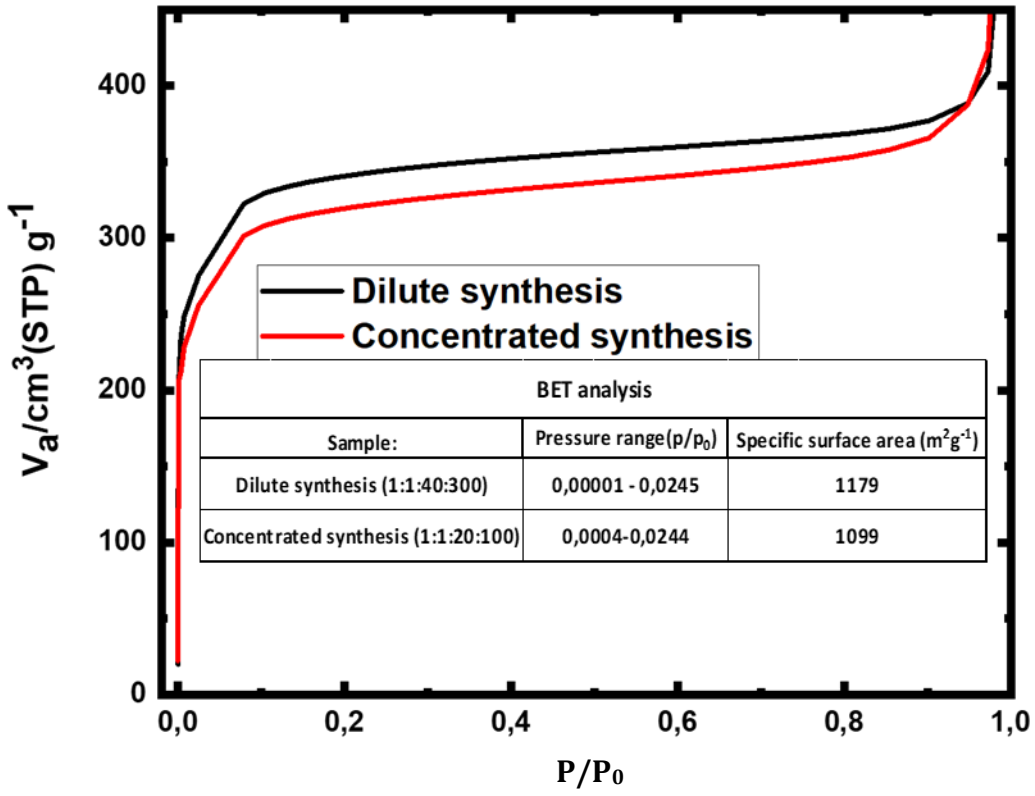

Figure 29: Comparison of the nitrogen adsorption isotherms for the dilute and concentrated samples obtained at −196 ℃. Table: specific BET surface area for both the dilute and concentrated samples.

From figure 29 its apparent that the sample from the concentrated synthesis have a lower specific BET surface area. It was therefore concluded that neither of the two samples contained missing cluster defects.

4.3.3. Controlling missing cluster defects

It is desired to control the missing cluster defects in a material. In the following experiment the A3 and B2 samples are reproduced. A third sample was also synthesized using the molar ratio of 1:1:25:150. This sample will be referred to as B2.5. This experiment is performed in order to investigate if the specific surface area of the material can be tuned using missing cluster defects.

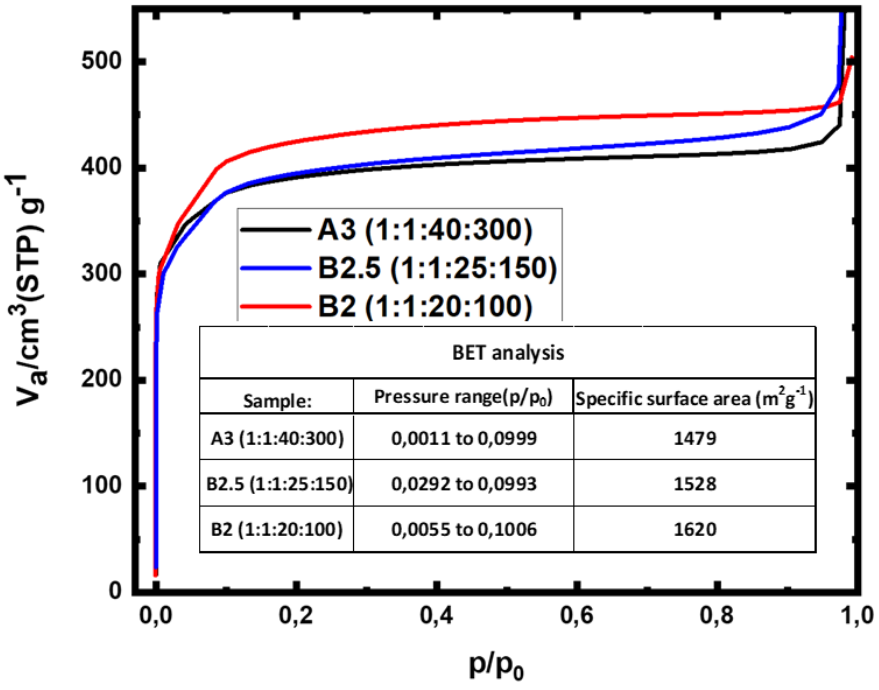

BET analysis		
Sample:	Pressure range(p/p_0)	Specific surface area (m^2g^{-1})
A3 (1:1:40:300)	0,0011 to 0,0999	1479
B2.5 (1:1:25:150)	0,0292 to 0,0993	1528
B2 (1:1:20:100)	0,0055 to 0,1006	1620

Figure 30: Comparison of the nitrogen adsorption isotherms for the A3, B2 and B2.5 sample obtained at −196 ℃. Table: specific BET surface area for A3, B2 and B2.5 samples.

Both the maximum uptake of nitrogen and the BET surface area increase as the synthesis is concentrated. The difference between A3 and B2.5 is relatively small. The increased surface area of the material is attributed to the formation of missing cluster defects. This experiment shows how the missing cluster defects and indirectly the surface area of the material can be tuned.

4.4. Changing the solvents

It has been shown that UiO-66 can be synthesized in a mixture of water and acetic acid using a hydrothermal approach [59]. Based on this work, similar experiments were performed for the 2,6-NDC MOF. In this thesis three different mixtures of DMF and water were used as solvent and each mixture was tested using four different concentrations of acetic acid. In this work the reflux synthesis procedure was applied. A summary of the molar ratios for the sample vials can be found in table 9.

Table 9: Summary of the molar ratios used in the solvent exchange synthesis. $ZrOCl_2 * 8H_2O$, linker, acetic acid, DMF and water are shown in black, red, green, light blue and dark blue respectively.

$ZrOCl_2*8H_2O$:Linker:Acetic acid:DMF:Water		
DS026A1	DS026B1	DS026C1
1:1:30:0:100	1:1:30:50:50	1:1:30:86:14
DS026A2	DS026B2	DS026C2
1:1:60:0:100	1:1:60:50:50	1:1:60:86:14
DS026A3	DS026B3	DS026C3
1:1:90:0:100	1:1:90:50:50	1:1:90:86:14
DS026A4	DS026B4	DS026C4
1:1:120:0:100	1:1:120:50:50	1:1:120:86:14

Especially four of these twelve samples were of great interest, DS026A1- DS026A3 and DS026C1. They will be discussed below.

4.4.1. DS026A1 – DS026A3 samples

The DS026A1 – DS026A3 samples are synthesized in pure water with no added DMF. A major concern for MOF synthesis in water is the often-low solubility of the linker, as is the case for the 2,6-NDC linker. It was therefore unexpected that the 2,6-NDC MOF would form under these synthesis parameters. To a great surprise a crystalline material was detected in the DS026A1- DS036A3 samples as shown in figure 31. The pXRD results of the 2,6-NDC linker is also shown in figure 31.

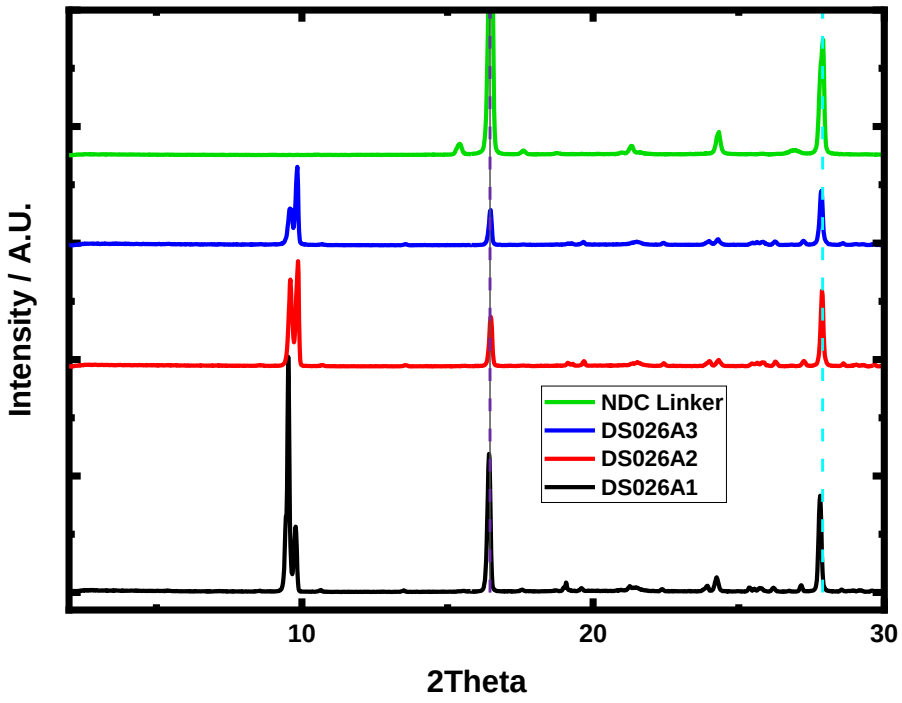

Figure 31: pXRD data obtained for DS026A1-DS026A3. The samples were mounted with plastic film. The plastic film diffracts at $2Theta$ = 20-22.

4.4.1.1. Structure elucidation

PXRD results for the DS026A1 - DS026A3 samples all showed indications of a crystalline material with a rather large unit cell indicated by a large peak at a low diffraction angle. Figure 31 suggests that excess linker is also present in the samples. DS026A1 was therefore washed with hot DMF to remove any excess linker. The washed diffractogram is illustrated in figure 32. The peak $2theta = 16{,}2$ are no longer observed in the pXRD pattern indicating that the excess of linker has been removed.

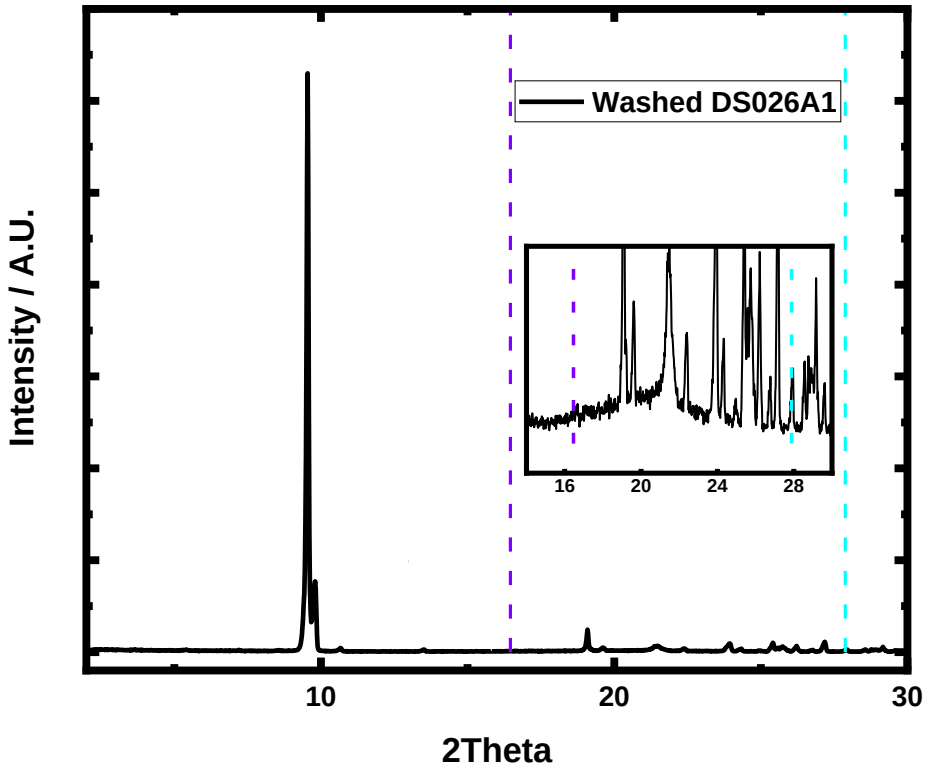

Figure 32: pXRD results obtained for DS026A1Washed. The sample was mounted with plastic film. The plastic film diffracts at $2Theta$ = 20-22.

The structure of the DS026A1 sample was elucidated using single crystal XRD. The structure is illustrated in figure 33 and the unit cell information is summarized in table 10.

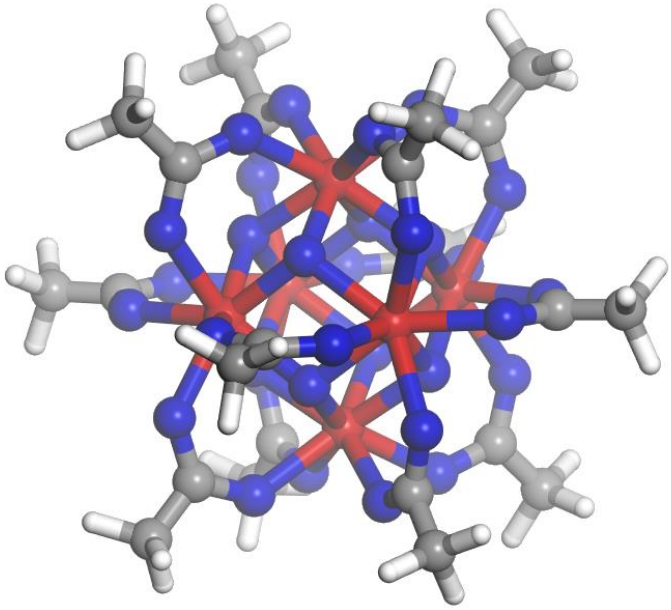

Figure 33: Illustration of the solved structure for DS026A1. The structure is best described as isolated zirconium clusters charge balanced by acetate ligands. Hydrogen illustrated by sticks for simplicity. Hydrogens at the cluster is omitted for clarity.

Table 10: Unit cell parameters for the solved structure of DS026A1.

Unit cell parameters for the solved structure	
Unit cell parameters:	**value:**
a	**12,5 Å**
b	**18,7 Å**
c	**18,5 Å**
Alpha	**90**
Beta	**90**
Gamma	**90**

The structure of the DS026A1 sample is best described as isolated zirconium clusters charge balanced by acetate. The zirconium clusters form a crystalline material because of weak forces between the clusters. The crystal system for the structure is orthorhombic. The space group is $Cmc2_1$. TGA and ^{1}H-NMR measurements were performed on the sample and are summarized in figure 34.

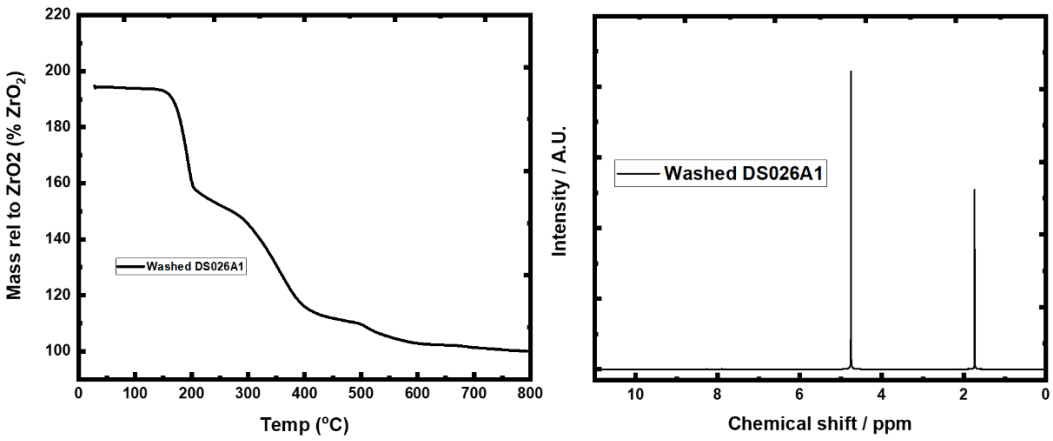

Figur 34: Left plot, solid line: normalized TGA results for Washed DS026A1. Right plot, ^{1}H-NMR spectrum for Washed DS026A1.

As expected, only acetate and water are detected by the ^{1}H-NMR measurement. The low thermal stability of the clusters is also expected as the clusters do not share any covalent bonds and only connected by weak Van der Waals forces.

The structure of the isolated acetate zirconium clusters has previously been reported in the literature [60]. The use of other charge balancing ligands than acetate have also been reported.

4.4.1.2. The intensity difference in the DS026A1-A3 samples

In figure 31, the DS026A1-A3 samples have two peaks at roughly $2theta = 9{,}8$. For DS026A1 the peak with the highest intensity is the peak at lower 2theta. For DS026A2 both the peaks are of similar intensity and for DS026A3 the peak at higher 2theta have the highest intensities. There are two explanations for this, first off, the samples could simply be different and therefore have different intensities. Secondly the topology of the sample could have a preferred orientation. A SEM experiment quickly confirmed that preferred orientation could be the reason for the intensity differences between the samples. Capillary pXRD was applied in order to remove preferred orientation.

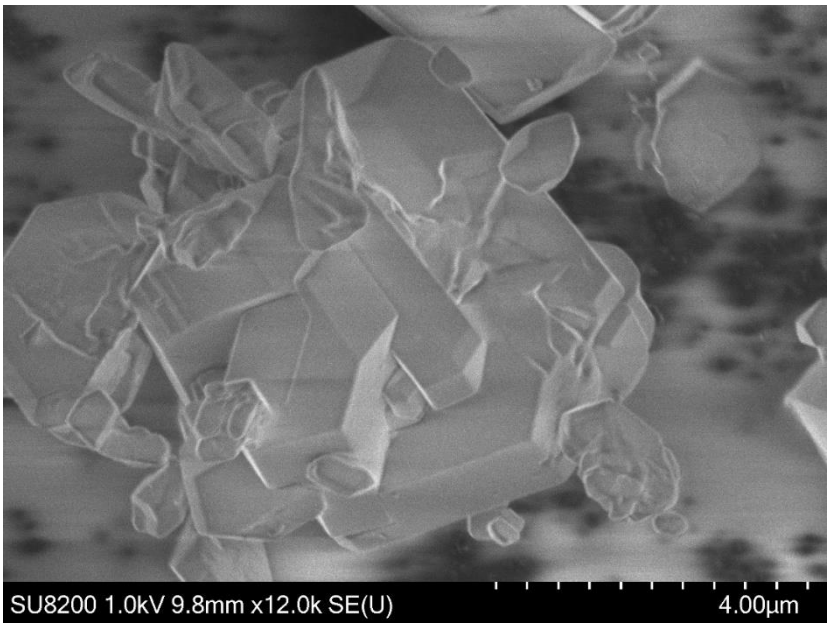

Figure 35: SEM image illustrating the topology of the Washed DS026A1 sample.

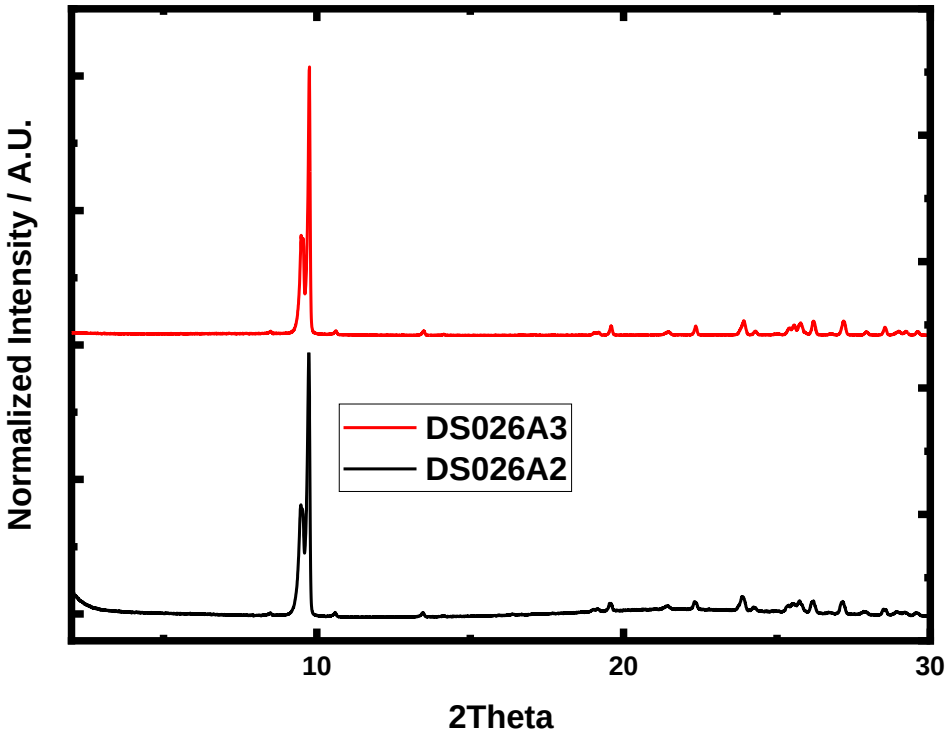

Figure 36: Illustration of capillary pXRD for DS026A2 and DS026A3. The illustrated capillary pXRD results are obtained on reproduced DS026A2 and DS026A3 samples.

The capillary pXRD results are shown in figure 36. The intensity of the peaks is now the same for DS026A2 and DS026A3 samples. The difference in intensity observed in the pXRD results shown in figure 31 was probably caused by preferred orientation of the crystallites.

The synthesis of these clusters has been reproduced without adding the linker and therefore also removing the necessity for the extra washing procedure. The synthesis procedure has not been tested for other charge compensating ligands such as formate.

4.4.2 DS026A1, DS026B1 and DS026C1

DS026A1 was synthesized water, DS026B1 and DS026C1 were synthesized in a 1:1 and 84:16 molar ratio of DMF and water respectively. The pXRD diffractograms of the three samples are shown in figure 37.

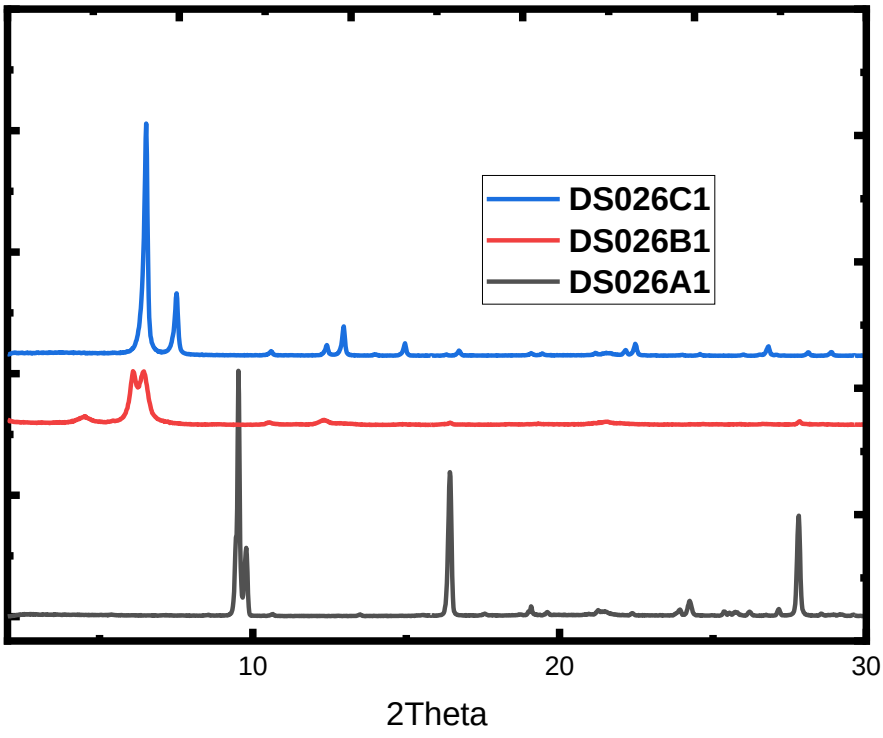

Figure 37: PXRD results for DS026A1 DS026B1 and DS026C1 samples. The structure of DS026A1 sample is isolated acetate zirconium clusters. The structure of DS026B1 is unknown and DS026C1 is the 2,6-NDC MOF. The samples were mounted with plastic film. The plastic film diffracts at $2theta$ = 20-22.

DS026A1 have been discussed thoroughly in the previous section. DS026B1 is a crystalline material with an unsolved structure, and DS026C1 is the 2,6-NDC MOF. The DS026C1 synthesis showcase that the 2,6-NDC MOF can still be synthesized after replacing 16 molar equivalents of DMF with water. This could be of great interest if the material is needed in a large scale.

4.5. Stability of zirconium MOF towards water

This section will focus on the stability of the 2,6-NDC MOF compared to UiO-66 and UiO-67 towards waters. It is well known in the literature that UiO-66 is more stable towards water than UiO-67. Fahra et al. published in 2019 an extensive paper where the reason behind UiO-66 superior stability over UiO-67 towards water, was investigated. In this work he investigates UiO-66, UiO-67, DUT – 52 (2,6-NDC MOF) and PCN – 57. They conclude that UiO-67 is the least stable MOF out of the four when considering thermal activation from different solvents. They believe the reason for the instability of UiO-67 towards water is caused by the angle of 15,8° between the carboxyl group and the phenyl ring [51]

In this work, the stability of UiO-66, UiO-67 and 2,6-NDC MOF from thermal activation after exposure to a high humidity will be investigated. The solvent exchange method will also be attempted. The experimental work is summarized in section 3.8.

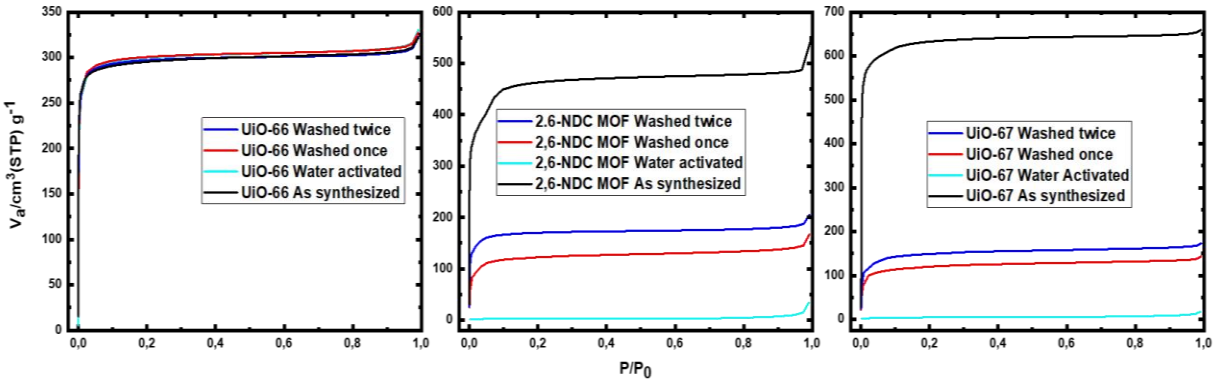

Figure 38: Left plot, comparison of the nitrogen adsorption isotherm for the UiO-66 as synthesized, UiO-66 Water activated, UiO-66 Washed once and UiO–66 Washed twice samples obtained at −196 ℃. Middle plot, similar as the left plot but for the 2,6-NDC MOF samples. Right plot, similar as the left plot but for the UiO-67 samples.

The BET analysis and the calculations are shown in Appendix D. From these nitrogen isotherms it is obvious that UiO-66 were the most stable MOF towards water. The surface area is unchanged by the treatments. The 2,6-NDC MOF completely loses its porosity when water is evaporated from the cavities. When the solvent exchanged method is applied, 28% of the porosity is retained. Performing the washing procedure twice increases the retained surface area to a total of 41 %.

UiO-67 also completely loses its porosity after activation from water. The washing procedure is far less rewarding for UiO-67 and only 18% and 22% of its porosity is retained after one and two washes respectively. UiO-67 is by far the least stable MOF toward water.

There are two main theories on framework collapse for zirconium MOFs when exposed to water. The fist theory suggests that the bonding between the zirconium and carboxylate group of the linker can be hydrolyzed [61]. The second theory suggests that strong capillary forces can result in framework collapse [50]. Both theories will be discussed below.

The hydrolysis theory suggests that the zirconium to linker bond may be hydrolyzed if water is able to access the bond. This theory offers a reasonable explanation for the superior stability of UiO-66. The organic linker of UiO-66 is shorter than the linker of 2,6-NDC MOF and UiO-67. A shorter linker result in a framework with narrower pores and smaller internal volume. The narrow pores of UiO-66 do not allow for significant access to the bond formed between zirconium and linker and can therefore not easily be hydrolyzed [61].

It has also been showed that the use of bulky linker in MOF synthesis can result in a more stable material towards water. Lillerud et al. reported that the use of linkers based on the bulky 3,3′-dimethylbiphenyl and 1,1′-binaphthyl scaffolds results in materials very stable towards water. This increased stability was attributed to the shielding of the carboxylate group and the adsorption site on the cluster [62].

Capillary force driven channel collapse was first proposed by Mondloch et al [50]. In this paper they argue that zirconium MOFs are stable towards hydrolysis of the zirconium linker bond. This was investigated by applying ls-NMR and spectroscopy to the filtrate of water soaked zirconium MOFs. Their results showed no trace of the linker molecule in the filtrate. They further argued that the thermal activation from a solvent with a large surface tension results in a collapsed framework. The surface area of the material is retained if the solvent inside the MOF is exchanged with a low surface tension solvent before the thermal activation.

A major difficulty of the capillary force theory is the size of microporous materials. It is well known that capillary forces can lead to collapse of porous materials such as aerogels [63]. It is also well documented in the literature that super critical drying is required in order to remove guest molecules of ultra porous MOFs without the loss of porosity. For UiO-66 the pore size is only 8 and 11 Å. It is often argued that a meniscus cannot be formed inside pores of 8 Å and 11 Å and therefore capillary forces cannot occur. This may also be the explanation for the higher stability of UiO-67 with bulky linkers. Bulky linkers occupy the volume of the pores and may inhibit the formation of a meniscus.

It could be possible that capillary forces can occur of on defect positions. Pores next to missing linker or missing cluster defects will be larger than the pores in the ideal structure. If these defect pores are large enough to accommodate the formation of a meniscus, capillary forces could occur. If this was the case, a study of UiO-66 samples with increasing concentration of defects should grant some insight.

The above discussion is just parts of the large discussion on the instability of many MOFs towards water. To date the difference in water sensitivity for zirconium MOFs are not known.

The pXRD results obtained on the same samples are showed and discussed below.

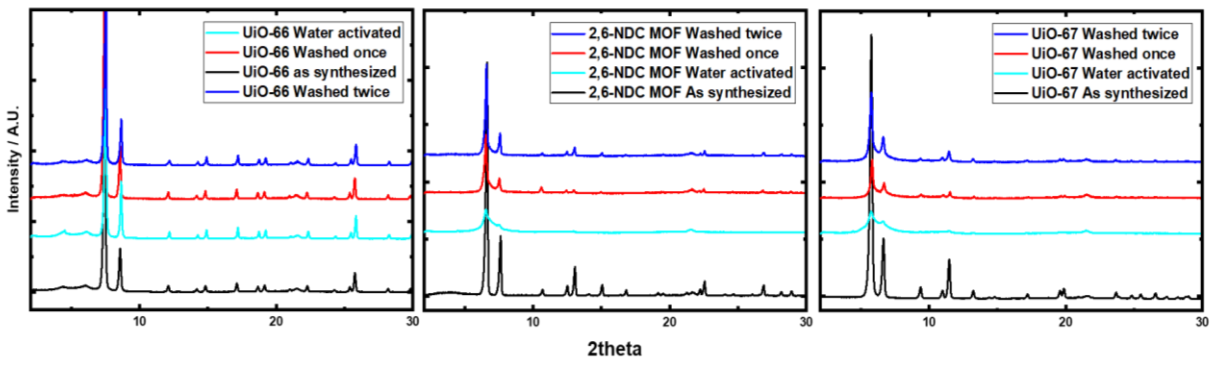

Figure 39: Left plot, comparison of the pXRD result for the UiO-66 as synthesized, UiO-66 Water activated, UiO-66 Washed once and UiO–66 Washed samples. Middle plot, similar as the left plot but for the 2,6-NDC MOF samples. Right plot, similar as the left plot but for the UiO-67 samples.

From figure 39 it is apparent that the treatments performed on the UiO-66 samples do not affect the sample to any significant extent. For 2,6-NDC MOF and UiO - 67 the evaporation of water from the cavities results in an almost completely amorphous material. The solvent exchange procedure seems work and some of the crystallinity of the samples are retained.

Nitrogen adsorption measurements are superior to pXRD measurements when comparing the degradation of the materials. It is simple to compare surface areas while comparing pXRD results are difficult.

5. Conclusion

In this thesis the zirconium 2,6-NDC MOF have been synthesized using a large array of methods. Both missing linker and missing cluster defects have been observed and characterized.

Missing linker defects in the 2,6-NDC MOF have been observed and characterized using TGA, ^{1}H-NMR and EDX. It has been derived how the combination of techniques could be used to quantitatively describe the defect situation. It has been demonstrated that linkers can be incorporated quantitatively by post-synthetic ligand exchange methods.

Missing cluster defects in the 2,6-NDC MOF have been observed in the 2,6-NDC MOF. The presence of missing cluster defects was determined using a combination of pXRD and nitrogen adsorption.

The water stability of 2,6-NDC MOF have been compared to the water stability of UiO-66 and UiO-67. As expected from the literature, the far most stable MOF is the UiO-66. 2,6-NDC MOF and UiO-67 both collapse when thermally activated with water inside the cavities. Comparing the behavior of the series of related materials UiO-66, UiO-67 and 2,6-NDC MOF have been utilized to discuss the validity of hypotheses that has been suggested in order to explain these surprising differences in water stability. By applying a post-synthetic solvent exchange with an organic solvent with a low surface tension, the framework could retain some of its original surface area.

6. Suggestion for further work

No functionalization of the linker or cluster were attempted in this thesis. To the best of the author knowledges, the only functionalization has been the addition of two hydroxyl group performed by Yaghi et al. As discussed in section 1.5. the naphthalene ring offers new and interesting chemistry in the field of MOF. Further work for the 2,6-NDC type MOF may be the incorporation of new and interesting functional groups. Especially the 1,8-bis(dimethylamino) naphthalene-2,6-dicarboxylic acid would be of great.

In this work it was showed that missing cluster defects could be incorporated into the framework by concentrating the synthesis. The presence of missing cluster defects could also be removed by using a solvothermal synthesis route. The same pattern was not observed for missing linker defects. No parameter(s) could be systematically changed in order to incorporate an increasing or decreasing quantity of missing linker defects. The reduction of missing linker defects could be achieved by increasing the linker to zirconium ratio during synthesis or performing a PSE. Both these procedures increase the usage of linker and results in an expansive synthesis route. It could be of interest to further investigate if the synthesis parameter(s) could be altered to allow for a systematical incorporating of missing linker defects.

References

1. Safaei, M., et al., *A review on metal-organic frameworks: Synthesis and applications.* Trends in Analytical Chemistry, 2019. **118**: p. 401-425.
2. Bai, Y., et al., *Zr-based metal–organic frameworks: design, synthesis, structure, and applications.* Chemical Society Reviews, 2016. **45**(8): p. 2327-2367.
3. Cavka, J.H., et al., *A New Zirconium Inorganic Building Brick Forming Metal Organic Frameworks with Exceptional Stability.* Journal of the American Chemical Society, 2008. **130**(42): p. 13850-13851.
4. Yaghi, O.M. and H. Li, *Hydrothermal Synthesis of a Metal-Organic Framework Containing Large Rectangular Channels.* Journal of the American Chemical Society, 1995. **117**(41): p. 10401-10402.
5. Liu, J., et al., *Applications of metal–organic frameworks in heterogeneous supramolecular catalysis.* Chemical Society Reviews, 2014. **43**(16): p. 6011-6061.
6. Li, H., et al., *Design and synthesis of an exceptionally stable and highly porous metal-organic framework.* Nature, 1999. **402**(6759): p. 276-279.
7. Sanda, S., S. Parshamoni, and S. Konar, *Third-Generation Breathing Metal–Organic Framework with Selective, Stepwise, Reversible, and Hysteretic Adsorption Properties.* Inorganic Chemistry, 2013. **52**(22): p. 12866-12868.
8. Kim, M., et al., *Postsynthetic ligand exchange as a route to functionalization of 'inert' metal–organic frameworks.* Chemical Science, 2012. **3**(1): p. 126-130.
9. Gutterød, E.S., et al., *CO2 Hydrogenation over Pt-Containing UiO-67 Zr-MOFs—The Base Case.* Industrial & Engineering Chemistry Research, 2017. **56**(45): p. 13206-13218.
10. Wu, H., et al., *Unusual and Highly Tunable Missing-Linker Defects in Zirconium Metal–Organic Framework UiO-66 and Their Important Effects on Gas Adsorption.* Journal of the American Chemical Society, 2013. **135**(28): p. 10525-10532.
11. Zhu, X., et al., *Inherent anchorages in UiO-66 nanoparticles for efficient capture of alendronate and its mediated release.* Chemical Communications, 2014. **50**(63): p. 8779-8782.
12. Taylor, J.M., et al., *Defect Control To Enhance Proton Conductivity in a Metal–Organic Framework.* Chemistry of Materials, 2015. **27**(7): p. 2286-2289.
13. *https://unfccc.int/process-and-meetings/the-paris-agreement/what-is-the-paris-agreement*. [cited 2020 27/05].
14. Li, L., et al., *High gas storage capacities and stepwise adsorption in a UiO type metal–organic framework incorporating Lewis basic bipyridyl sites.* Chemical Communications, 2014. **50**(18): p. 2304-2307.
15. Wang, B., et al., *Tuning CO2 Selective Adsorption over N2 and CH4 in UiO-67 Analogues through Ligand Functionalization.* Inorganic Chemistry, 2014. **53**(17): p. 9254-9259.
16. Furukawa, H., et al., *Water Adsorption in Porous Metal–Organic Frameworks and Related Materials.* Journal of the American Chemical Society, 2014. **136**(11): p. 4369-4381.
17. Shearer, G., *On the defect chemistry of metal-organic framework compound UiO-66.* 2016.
18. Chui, S.S., et al., *A chemically functionalizable nanoporous material.* Science, 1999. **283**(5405): p. 1148-50.
19. Férey, G., et al., *A chromium terephthalate-based solid with unusually large pore volumes and surface area.* Science, 2005. **309**(5743): p. 2040-2.
20. He, T., et al., *Fast and scalable synthesis of uniform zirconium-, hafnium-based metal–organic framework nanocrystals.* Nanoscale, 2017. **9**(48): p. 19209-19215.
21. Kirchon, A., et al., *From fundamentals to applications: a toolbox for robust and multifunctional MOF materials.* Chemical Society Reviews, 2018. **47**(23): p. 8611-8638.

22. Yuan, S., et al., *Stable Metal–Organic Frameworks: Design, Synthesis, and Applications*. 2018. p. n/a-n/a.
23. Valenzano, L., et al., *Disclosing the Complex Structure of UiO-66 Metal Organic Framework: A Synergic Combination of Experiment and Theory.* Chemistry of Materials, 2011. **23**(7): p. 1700-1718.
24. Øien, S., *Preparation, structure and reactivity of functionalized zirconium metal-organic frameworks.* 2016.
25. amedjkouh, M., *Lecture: 09 - Substitution 2019.*
26. Øien, S., et al., *Detailed Structure Analysis of Atomic Positions and Defects in Zirconium Metal–Organic Frameworks.* Crystal Growth & Design, 2014. **14**(11): p. 5370-5372.
27. Bon, V., et al., *Tailoring of network dimensionality and porosity adjustment in Zr- and Hf-based MOFs.* CrystEngComm, 2013. **15**(45): p. 9572-9577.
28. Flaig, R.W., et al., *The Chemistry of CO2 Capture in an Amine-Functionalized Metal–Organic Framework under Dry and Humid Conditions.* Journal of the American Chemical Society, 2017. **139**(35): p. 12125-12128.
29. Benoit, R.L., D. Lefebvre, and M. Fréchette, *Basicity of 1,8-bis(dimethylamino)naphthalene and 1,4-diazabicyclo[2.2.2]octane in water and dimethylsulfoxide.* Canadian Journal of Chemistry, 1987. **65**(5): p. 996-1001.
30. Shearer, G.C., et al., *Tuned to Perfection: Ironing Out the Defects in Metal–Organic Framework UiO-66.* Chemistry of Materials, 2014. **26**(14): p. 4068-4071.
31. Cliffe, M.J., et al., *Correlated defect nanoregions in a metal–organic framework.* Nature Communications, 2014. **5**(1): p. 4176.
32. Shearer, G.C., et al., *Defect Engineering: Tuning the Porosity and Composition of the Metal–Organic Framework UiO-66 via Modulated Synthesis.* Chemistry of Materials, 2016. **28**(11): p. 3749-3761.
33. Koutsianos, A., et al., *A new approach to enhancing the CO2 capture performance of defective UiO-66 via post-synthetic defect exchange.* Dalton Transactions, 2019. **48**(10): p. 3349-3359.
34. Schaate, A., et al., *Modulated Synthesis of Zr-Based Metal–Organic Frameworks: From Nano to Single Crystals.* Chemistry – A European Journal, 2011. **17**(24): p. 6643-6651.
35. *http://pd.chem.ucl.ac.uk/pdnn/powintro/planes.htm*. [cited 2020 28/05].
36. *https://www.tandfonline.com/doi/full/10.1080/10408347.2014.949616*. [cited 2020 28/05].
37. *http://pd.chem.ucl.ac.uk/pdnn/inst1/mounts.htm*. [cited 2020 28/05].
38. *http://pd.chem.ucl.ac.uk/pdnn/inst1/texture1.htm*. [cited 2020 28/05].
39. Wragg, D., *Basic XRD, pXRD training 2018.*
40. Sjåstad, A., *Thermodynamics_KJM-MENA3120_2019_Thermal analysis methods_Lectures 4-5 2019.*
41. Sjåstad, A., *Lecture Notes Topic 2 2019.*
42. Svelle, S., *02 - porous materials and adsorption methods and hysteresis, 2019.*
43. Rouquerol, J., P. Llewellyn, and F. Rouquerol, *Is the BET Equation Applicable to Microporous Adsorbents?* Studies in Surface Science and Catalysis, 2007. **160**: p. 49-56.
44. Gómez-Gualdrón, D.A., et al., *Application of Consistency Criteria To Calculate BET Areas of Micro- And Mesoporous Metal–Organic Frameworks.* Journal of the American Chemical Society, 2016. **138**(1): p. 215-224.
45. *https://www.3dsbiovia.com/products/datasheets/sorption.pdf*. [cited 2019 19/06].
46. https://www.naturfag.no/artikkel/vis.html?tid=686155. [cited 2020 25/03].
47. *http://nmrweb.chem.ox.ac.uk/Data/Sites/70/userfiles/pdfs/quantitative-nmr.pdf*. [cited 2020 23/05].
48. *https://www.thermofisher.com/blog/microscopy/what-is-sem-scanning-electron-microscopy-explained/*. [cited 2020 28/05].

49. https://blog.phenom-world.com/edx-analysis-sem. [cited 2020 28/05].
50. Mondloch, J.E., et al., *Are Zr6-based MOFs water stable? Linker hydrolysis vs. capillary-force-driven channel collapse.* Chemical Communications, 2014. **50**(64): p. 8944-8946.
51. Ayoub, G., et al., *Torsion Angle Effect on the Activation of UiO Metal–Organic Frameworks.* ACS Applied Materials & Interfaces, 2019. **11**(17): p. 15788-15794.
52. Taddei, M., et al., *Post-Synthetic Ligand Exchange in Zirconium-Based Metal-Organic Frameworks: Beware of The Defects!* Angew Chem Int Ed Engl, 2018. **57**(36): p. 11706-11710.
53. Harrison, R.L., *Introduction To Monte Carlo Simulation.* AIP conference proceedings, 2010. **1204**: p. 17-21.
54. Schmitz-Antoniak, C. and M. Farle, *Magnetism at the nanoscale: The case of FePt.* Modern Physics Letters B, 2007. **21**: p. 1111.
55. Burrows, A.D., et al., *Solvent hydrolysis and templating effects in the synthesis of metal–organic frameworks.* CrystEngComm, 2005. **7**(89): p. 548-550.
56. https://www.malvernpanalytical.com/en/products/technology/microcalorimetry/differential-scanning-calorimetry. [cited 2020 28/05].
57. Mohamed, S.A., S. Chong, and J. Kim, *Thermal Stability of Methyl-Functionalized MOF-5.* The Journal of Physical Chemistry C, 2019. **123**(49): p. 29686-29692.
58. Kaur, G., et al., *Controlling the Synthesis of Metal–Organic Framework UiO-67 by Tuning Its Kinetic Driving Force.* Crystal Growth & Design, 2019. **19**(8): p. 4246-4251.
59. Hu, Z., et al., *A Modulated Hydrothermal (MHT) Approach for the Facile Synthesis of UiO-66-Type MOFs.* Inorganic Chemistry, 2015. **54**(10): p. 4862-4868.
60. Hennig, C., et al., *Solution Species and Crystal Structure of Zr(IV) Acetate.* Inorganic Chemistry, 2017. **56**(5): p. 2473-2480.
61. DeCoste, J.B., et al., *Stability and degradation mechanisms of metal–organic frameworks containing the Zr6O4(OH)4 secondary building unit.* Journal of Materials Chemistry A, 2013. **1**(18): p. 5642-5650.
62. Øien-Ødegaard, S., et al., *UiO-67-type Metal–Organic Frameworks with Enhanced Water Stability and Methane Adsorption Capacity.* Inorganic Chemistry, 2016. **55**(5): p. 1986-1991.
63. Herman, T., J. Day, and J. Beamish, *Deformation of silica aerogel during fluid adsorption.* Physical Review B, 2006. **73**(9): p. 094127.

Appendix

A: Calculating the formula mass of 2,6-NDC MOF

The chemical formula of ideal hydroxylated 2,6-NDC MOF is $Zr_6O_4(OH)_4(C_{12}O_4H_6)_6$. Table 40 summarize the amount of each element, the molecular mass of each element and as the total mass.

Table 11: Overview of all the elements of ideal 2,6-NDC

Element:	Number of each element(#):	Molecular weight of each element (g/mol):	Total mass (g/mol):
Zirconium	6	91,22	547,3
Oxygen	32	15,99	511,7
Carbon	72	12,01	864,7
Hydrogen	40	1,007	40,28
Formula mass of 2,6 - NDC MOF:			1964

The molecular weight of ideal 2,6-NDC MOF is 1964 $\frac{g}{mol}$.

The molecular weight of ideal 2,6-NDC MOF with dehydroxylated clusters is 1928 $\frac{g}{mol}$.

B: Calculating the formula mass of a unit cell of 2,6-NDC MOF

The number of each element inside a unit cell of 2,6-NDC MOF could easily be found by importing the CIF file of 2,6-NDC MOF.

Table 12: Overview of all the elements of the unit cell of ideal 2,6-NDC

Element:	Number of each element(#):	Molecular weight of each element (g/mol):	Total mass (g/mol):
Zirconium	24	91,22	2189,3
Oxygen	128	15,99	2046,7
Carbon	288	12,01	3458,9
Hydrogen	144	1,007	145,01
Formula mass of the unit cell of 2,6 - NDC MOF:			7839,888

C: Unit transformation of simulated values

The unit of simulated nitrogen adsorption isotherms from material studios are total fugacity (KPa) and nitrogen adsorbed per unit cell. The experimental determined values are given in units Prel (unitless) and volume adsorbed nitrogen ($\frac{cm^3}{g}$) at standard condition. In order to transform the units for the simulated values to the units of the experimentally determined, equation 11 and equation 12 can be applied [17].

$$\boldsymbol{Relative\ pressure}\ \left(\frac{\boldsymbol{p}}{\boldsymbol{p^0}}\right) = \frac{\boldsymbol{Total\ fugacity\ (kPa)}}{\boldsymbol{Atmosphere\ pressure\ (kPa)}} \tag{11}$$

$$\boldsymbol{V_a}\left(\frac{\boldsymbol{cm^3(STP)}}{\boldsymbol{G}}\right) = \frac{\boldsymbol{N_2\ Molecules\ per\ unit\ cell}}{\boldsymbol{M_{unit\ cell}}} * \frac{\boldsymbol{RT}}{\boldsymbol{P}} \tag{12}$$

Where:

$\boldsymbol{V_a}$ is the volume adsorbed nitrogen at standard condition per gram.

$\boldsymbol{N_2\ Molecules\ per\ unit\ cell}$ is the adsorbed nitrogen per unit cell.

$\boldsymbol{R}$ is the universal gas constant.

$\boldsymbol{T}$ is is the standard temperature.

$\boldsymbol{P}$ is the standard pressure.

D: Specific surface area for the samples section 4.5.

Table 13: Overview of the BET specific surface area for all the samples presented in section 4.5.

BET analysis		
Sample:	**Pressure range (p/p_0)**	**Specific surface area (m^2g^{-1})**
UiO-66 As synthesized	0,00003909 - 0,029776	1202
UiO-66 Water activated	0,000157-0,0282	1215
UiO - 66 Washed Once	0,00024 - 0,0246	1220
UiO - 66 Washed twice	0,00379 - 0,02826	1221
2,6-NDC MOF As synthesized	0,00449 - 0,0368	1665
2,6-NDC MOF Water activated	0,0019-0,054	11
2,6-NDC MOF once washed	0,00108 - 0,07644	474
2,6-NDC MOF twice washed	0,00507 - 0,05116	682
UiO-67 As synthesized	0,000983 - 0,0407	2527
UiO-67 Water activated	0,00189-0,13	17
UiO-67 Washed once	0,001 - 0,07657	458
UiO -67 Washed twice	0,00028 - 0,05021	556

Calculation of the retained surface area are exemplified for UiO-67 Water activated

Retained surface area for UiO-67 Water activated

$$\frac{17\,\frac{m^2}{g}}{2527\,\frac{m^2}{g}} * 100\ \% = 0{,}67\ \%$$

0,67 % of the surface area is retained for the UiO-67 Water activated sample.